

Spatial distribution of interstellar gas in the innermost 3 kpc of our Galaxy

K. Ferrière¹, W. Gillard², and P. Jean²

¹ LATT-OMP, CNRS/UPS, 31028 Toulouse Cedex 4, France

² CESR-OMP, CNRS/UPS, B.P. 4346, 31028 Toulouse Cedex 4, France

Received ; accepted

ABSTRACT

Aims. We review the present observational knowledge on the spatial distribution and the physical state of the different (molecular, atomic and ionized) components of the interstellar gas in the innermost 3 kpc of our Galaxy – a region which we refer to as the interstellar Galactic bulge, to distinguish it from its stellar counterpart.

Methods. We try to interpret the observations in the framework of recent dynamical models of interstellar gas flows in the gravitational potential of a barred galaxy.

Results. Relying on both the relevant observations and their theoretical interpretation, we propose a model for the space-averaged density of each component of the interstellar gas in the interstellar Galactic bulge.

Key words. ISM: general - ISM: structure - ISM: kinematics and dynamics - Galaxy: bulge - Galaxy: structure - Galaxy: kinematics and dynamics

1. Introduction

The state of knowledge on the Galactic center (GC) environment prevailing one decade ago was reviewed independently by Morris & Serabyn (1996) and by Mezger et al. (1996). To summarize the main points relevant to our work, the Galactic bulge (GB) is the region of our Galaxy inside Galactocentric radius $r \simeq 3$ kpc – a radius which roughly corresponds to the inner boundary of the Galactic disk molecular ring. The outer parts of the GB, outside $r \sim 1.5$ kpc, are largely devoid of interstellar gas. Atomic gas is confined to a noticeably tilted layer extending (in projection) out to $r \sim 1.5$ kpc (Burton & Liszt 1978; Liszt & Burton 1980). This H I layer is sometimes referred to as the H I nuclear disk (Morris & Serabyn 1996), but we find this denomination misleading, as we think that the term “nuclear” should be reserved to objects and regions with smaller Galactic radii (e.g., $r \lesssim 300$ pc, the approximate radius of the nuclear bulge). For want of any better term, we will refer to this H I layer as the H I GB disk. The GB disk also includes significant amounts of H₂, whose general distribution and kinematics were argued to be similar to those of H I (Liszt & Burton 1978; Burton & Liszt 1992; but see also Sanders et al. 1984; Combes 1991 for a different viewpoint). However, molecular gas tends to concentrate in the so-called central molecular zone (CMZ), an asymmetric layer of predominantly molecular gas extending (in projection) out to $r \sim 200$ pc – more exactly, $r \sim 250$ pc at positive longitudes and $r \sim 150$ pc at negative longitudes. The CMZ itself contains a ring-like feature with mean radius ~ 180 pc, now known as the 180-pc molecular ring, and, deeper inside, a thin sheet populated by dense molecular clouds, known as the GC disk population or the GC molec-

ular disk (Bally et al. 1987, 1988). The observed kinematics of the 180-pc molecular ring indicate strongly non-circular motions, which in turn suggest that either the ring is radially expanding (Kaifu et al. 1972; Scoville 1972; hence the historically often used denomination of “expanding molecular ring”) or, more likely, that the gas travels along highly elongated orbits (e.g., Bally et al. 1988; Binney et al. 1991).

A number of significant advances were made in the last decade, which contributed to improving our knowledge and understanding of the interstellar GB. Nonetheless, several aspects remain ambiguous or controversial, and important pieces of the puzzle are still missing, mainly due to the severe interstellar extinction along the line of sight to the GC, to the existence of strongly non-circular motions and to the lack of accurate distance information. Thus, to date, no complete and fully consistent picture has emerged from the vast body of existing observational data.

In this paper, we put together a model for the spatial distribution of interstellar gas in the Galactic region $r \lesssim 3$ kpc, based on the observational results summed up by Morris & Serabyn (1996) and Mezger et al. (1996), on more recent observational studies of dust thermal emission, CO line emission, H I 21-cm line emission and absorption and pulsar dispersion measures, and on recent theoretical investigations of interstellar gas dynamics near the GC. Our model complements that developed by Ferrière (1998, 2001) for the Galactic disk outside $r \simeq 3$ kpc. In section 2, we review the observations pertaining to the spatial distribution and the physical state of interstellar gas in its molecular, atomic and ionized forms. In section 3, we discuss a few dynamical models of interstellar gas subject to the barred gravitational potential of the Galaxy, and we make the link between the theoretical predictions of these models and the observational facts reviewed in section 2. In section 4, we

reconcile as well as possible the disparate observational and theoretical results presented in the preceding sections, and we incorporate them into a new, consistent model for the space-averaged density of interstellar gas in the Galactic region $r \lesssim 3$ kpc. In section 5, we conclude our study.

For consistency with Ferrière (1998, 2001) and in line with most papers discussed below, the Sun is assumed to lie at a distance $r_{\odot} = 8.5$ kpc from the GC,¹ even though recent work favors a somewhat smaller value. All spatial distributions will be given either as functions of Galactocentric cartesian coordinates (x, y, z) , with the x -axis pointing toward the Sun, the y -axis in the direction $l = +90^\circ$ and the z -axis toward the North Galactic Pole (NGP), or as functions of Galactocentric cylindrical coordinates (r, θ, z) , with θ increasing in the direction of Galactic rotation, i.e., clockwise as seen from the NGP (see Figure 1). Toward the vicinity of the GC, $y \simeq (150 \text{ pc}) (l/1^\circ)$ and $z \simeq (150 \text{ pc}) (b/1^\circ)$, where as usual l and b denote Galactic longitude and latitude, respectively. Finally, the projected (onto the plane of the sky) horizontal distance from the GC is given by $r_{\perp} = |y| \simeq (150 \text{ pc}) (|l|/1^\circ)$.

2. Observational overview

In this section, we successively review the current observational status of the total interstellar matter (section 2.1), the molecular gas (section 2.2), the atomic gas (section 2.3) and the ionized gas (section 2.4). For each, we provide quantitative estimates for the space-averaged density and the mass of interstellar hydrogen in subregions of the GB. The density and mass of the total interstellar matter (including helium and metals) immediately follow, once the interstellar elemental abundances in the GB are known.

Various lines of evidence, primarily from HII regions (Shaver et al. 1983; Afflerbach et al. 1997), planetary nebulae (Maciel & Quireza 1999) and early B-type stars (Rolleston et al. 2000), converge to point to the existence of an inward metallicity gradient $\sim (0.06 - 0.07) \text{ dex kpc}^{-1}$ in the inner Galactic disk. If extrapolated in to the GC, this metallicity gradient implies an increase in metallicity by a factor $\sim 3 - 4$ between the Sun and the GC. On the other hand, direct abundance measurements near the GC yield mixed results : while some confirm the high metallicity predicted for the GC region (e.g., Smartt et al. 2001), others indicate instead a close-to-solar metallicity (e.g., Carr et al. 2000; Najarro et al. 2004). Here, we adopt the intermediate, and rather conservative, value $Z_{\text{GC}} = 2 Z_{\odot}$ for the GC metallicity (as in Launhardt et al. 2002, and consistent with Sodroski et al. 1995; see below). Furthermore, since the measured He^+/H^+ ratio does not exhibit any significant radial gradient (Shaver et al. 1983), we adopt $Y_{\text{GC}} = Y_{\odot}$ for the GC helium fraction. Altogether, with a helium-to-hydrogen mass ratio of 0.4 and a metal-to-hydrogen mass ratio of 2×0.0265 (see, e.g., Anders & Grevesse 1989; Däppen 2000), the conversion factor from interstellar hydrogen masses to total interstellar masses is 1.453.

¹ All our estimates can easily be rescaled to any other value of r_{\odot} : distances scale as r_{\odot} , surface densities as r_{\odot}^0 , volume densities as r_{\odot}^{-1} and masses as r_{\odot}^2 .

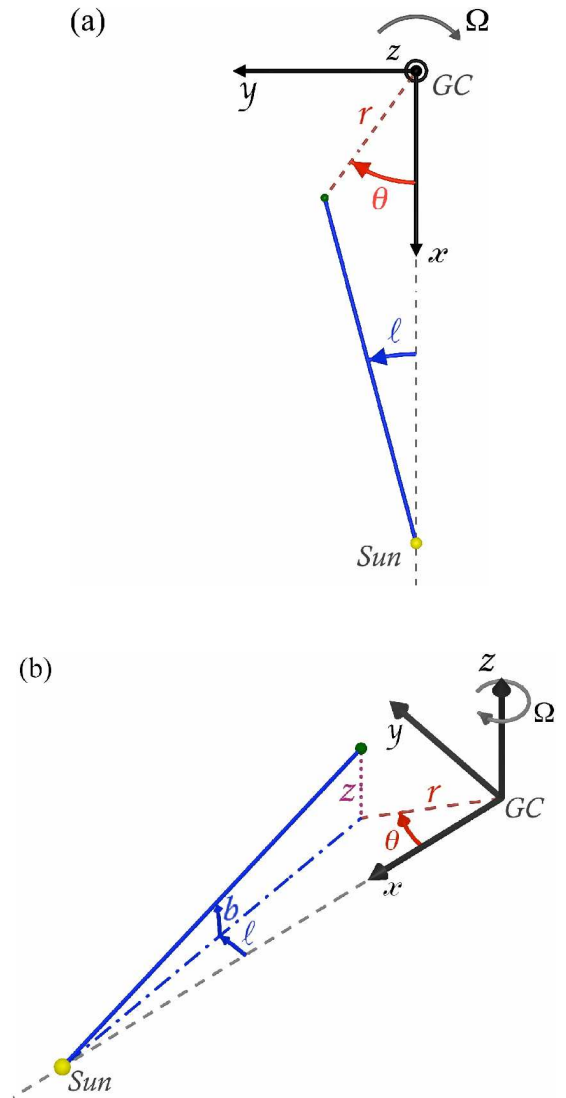


Fig. 1. The (x, y, z) and (r, θ, z) Galactocentric coordinate systems used in the present paper: (a) two-dimensional view looking down from the NGP; (b) full three-dimensional view. Note that both systems must be left-handed if one wants to stick to the usual conventions that z has the same sign as b (i.e., positive/negative in the northern/southern Galactic hemisphere) and that θ increases in the direction of Galactic rotation (i.e., clockwise about the z -axis).

2.1. Total interstellar matter in the innermost 500 pc

The large-scale spatial distribution of interstellar matter in the CMZ was derived by Launhardt et al. (2002), based on IRAS and COBE/DIRBE far-infrared maps of the central kpc of the Galaxy. They converted the optically thin $240 \mu\text{m}$ dust emission map into a hydrogen column density map, using for the dust temperature an empirical color temperature proportional to the $60\text{-to-}140 \mu\text{m}$ flux ratio and for the H-to-dust mass ratio the standard value near the Sun, $(M_{\text{H}}/M_{\text{d}})_{\odot} = 110$, divided by the relative metallicity, $(Z_{\text{GC}}/Z_{\odot}) = 2$.

In contrast to previous authors, Launhardt et al. (2002) defined the CMZ as the entire region interior to $r \sim 500$ pc, and they divided it into the inner CMZ, physically associated with the stellar nuclear bulge ($r \lesssim 230$ pc) and heated

Table 1. Estimated values of the mass of interstellar hydrogen (in any form) in specific regions of the GB.

Region of space	Radial range	Hydrogen mass	Reference
Inner CMZ : inner disk	$\simeq 0 - 120$ pc	$\sim 4 \times 10^6 M_\odot$	Launhardt et al. (2002)
outer torus	$\simeq 130$ pc – 230 pc	$\sim 1.6 \times 10^7 M_\odot$	"
Outer CMZ : $l > 0^\circ$	~ 230 pc – 500 pc	$\sim 2.9 \times 10^7 M_\odot$	"
$l < 0^\circ$		$\sim 1.1 \times 10^7 M_\odot$	"
Entire CMZ	$\sim 0 - 500$ pc	$\sim 6 \times 10^7 M_\odot$	"

by its stars, and the outer CMZ, containing dust too cold to be possibly heated by stars from the nuclear bulge.

Extinction arguments as well as comparisons with high-resolution submm continuum maps led Launhardt et al. (2002) to conclude that interstellar matter in the nuclear bulge is extremely clumpy. According to them, $\gtrsim 90\%$ of the interstellar matter would be trapped in small, compact molecular clouds occupying only a few % of the interstellar volume. The average hydrogen density inside these clouds would, therefore, be \sim a few 10^3 cm^{-3} , with possibly much higher values in the cloud cores. The remaining $\lesssim 10\%$ of the interstellar matter would form a diffuse, homogeneously distributed intercloud medium, Launhardt et al. (2002) further divided the inner CMZ into a warm inner disk with radius $\simeq 120$ pc and a cold outer torus centered on the 180-pc molecular ring and extending radially between $\simeq 130$ pc and 230 pc. The whole disk/torus structure has a FWHM thickness $\simeq 45$ pc and a total hydrogen mass $\sim 2.0 \times 10^7 M_\odot$, with $\sim 4 \times 10^6 M_\odot$ in the inner disk and $\sim 1.6 \times 10^7 M_\odot$ in the outer torus. The space-averaged density of hydrogen nuclei can be approximated by²

$$\langle n_{\text{H}} \rangle_{\text{disk}}(r, z) = (72 \text{ cm}^{-3}) \exp \left[- \left(\frac{r - 70 \text{ pc}}{L} \right)^4 \right] \times \exp \left[- \left(\frac{|z|}{H} \right)^{1.4} \right] \quad (1)$$

in the inner disk and

$$\langle n_{\text{H}} \rangle_{\text{torus}}(r, z) = (106 \text{ cm}^{-3}) \exp \left[- \left(\frac{r - 180 \text{ pc}}{L} \right)^4 \right] \times \exp \left[- \left(\frac{|z|}{H} \right)^{1.4} \right] \quad (2)$$

in the outer torus, with $L = (100 \text{ pc}) / (2 (\ln 2)^{1/4}) \simeq 55$ pc and $H = (45 \text{ pc}) / (2 (\ln 2)^{1/1.4}) \simeq 29$ pc. Note that strictly speaking, Equation 1 implies that the inner disk extends radially between $\simeq 20$ pc and 120 pc, whereas the actual matter distribution is likely to continue in to the origin; but since the region $r \lesssim 20$ pc contributes very little to the total mass, this approximation is perfectly valid.

Launhardt et al. (2002) also found large amounts of interstellar dust too cold to belong to the nuclear bulge, although its projected distribution onto the plane of the sky would place most of this dust inside the nuclear bulge. The associated interstellar hydrogen has a mass $\sim 2.9 \times 10^7 M_\odot$ at positive longitudes ($0.5^\circ \leq l \leq 4^\circ$) and $\sim 1.1 \times 10^7 M_\odot$

at negative longitudes ($-4^\circ \leq l \leq -2^\circ$). It could be this interstellar matter, located in the outer CMZ, that would be responsible for the observed asymmetry of the CMZ. Altogether, the total mass of interstellar hydrogen enclosed within the central kpc of the Galaxy is $\sim 6 \times 10^7 M_\odot$ (see Table 1).

with an average hydrogen density $\sim 10 \text{ cm}^{-3}$, and the strong UV radiation field from the numerous high-mass stars embedded in the nuclear bulge would cause this thin intercloud medium to be both warm and ionized. As will become apparent in the course of this section, the two above density estimates are compatible with more direct density estimates for molecular gas (see section 2.2) and for ionized gas (see section 2.4).

2.2. Molecular gas

Radio emission lines of interstellar molecules (excluding H_2 , which possesses no permitted lines at radio frequencies) constitute one of the best tools to probe interstellar molecular gas in remote Galactic regions, and chief amongst them is the ^{12}CO ($J = 1 \rightarrow 0$) line at 2.6 mm. Unfortunately, the ^{12}CO ($J = 1 \rightarrow 0$) line as a tracer of molecular gas is plagued by the considerable uncertainty in the ^{12}CO -to- H_2 conversion factor, X_{CO} , which relates the H_2 column density, N_{H_2} , to the velocity-integrated intensity of the ^{12}CO line, $W_{^{12}\text{CO}}$, through $N_{\text{H}_2} = X_{\text{CO}} W_{^{12}\text{CO}}$.

Sodroski et al. (1995) estimated the value of X_{CO} near the GC by combining the Goddard-Columbia surveys of ^{12}CO ($J = 1 \rightarrow 0$) emission with COBE/DIRBE observations at $140 \mu\text{m}$ and $240 \mu\text{m}$. To deduce the H_2 column density from the far-infrared data, they assumed that the gas-to-dust mass ratio is inversely proportional to metallicity, Z , and that Z is ~ 1.5 – 3 times higher near the GC than in the inner Galactic disk ($2 \text{ kpc} \lesssim r \lesssim 7 \text{ kpc}$). Accordingly, they found that X_{CO} is ~ 3 – 10 times lower near the GC than in the inner Galactic disk, which, together with $X_{\text{CO}} \sim 2.2 \times 10^{20} \text{ cm}^{-2} \text{ K}^{-1} \text{ km}^{-1} \text{ s}$ in the inner Galactic disk, leads to $X_{\text{CO}} \sim (2-7) \times 10^{19} \text{ cm}^{-2} \text{ K}^{-1} \text{ km}^{-1} \text{ s}$ near the GC. The corresponding H_2 mass inside the longitude range $-1.5^\circ \leq l \leq 3.5^\circ$ (projected half-size $\simeq 375$ pc) is then $\sim (2-6) \times 10^7 M_\odot$.

Arimoto et al. (1996) studied the radial dependence of the conversion factor in more detail, by comparing the CO luminosities to the virial masses of a large number of giant molecular clouds situated at various distances from the GC. In this manner, they obtained the relation (rescaled to $r_\odot = 8.5 \text{ kpc}$)

$$X_{\text{CO}}(r) \sim (9 \times 10^{19} \text{ cm}^{-2} \text{ K}^{-1} \text{ km}^{-1} \text{ s}) \exp \left(\frac{r}{7.1 \text{ kpc}} \right). \quad (3)$$

Note in passing that Equation 3 implies $X_{\text{CO}}(r_\odot) \sim 3 \times 10^{20} \text{ cm}^{-2} \text{ K}^{-1} \text{ km}^{-1} \text{ s}$.

² The space-averaged densities given by Launhardt et al. (2002) must be divided by a factor of 3.5 in order to match the masses and column densities quoted in their paper (Launhardt, private communication).

Table 2. Estimated values of the ^{12}CO -to- H_2 conversion factor, $X_{\text{CO}} = N_{\text{H}_2}/W_{^{12}\text{CO}}$ (expressed in $\text{cm}^{-2} \text{K}^{-1} \text{km}^{-1} \text{s}$), both near the GC ($r \sim 0$) and either in the inner Galactic disk ($r \simeq 2 - 7 \text{ kpc}$) or in the vicinity of the Sun ($r \sim r_\odot$).

$X_{\text{CO}}(r \sim 0)$	$X_{\text{CO}}(r \simeq 2 - 7 \text{ kpc})$	$X_{\text{CO}}(r \sim r_\odot)$	Reference
$\sim (2 - 7) \times 10^{19}$	$\sim 2.2 \times 10^{20}$		Sodroski et al. (1995)
$\sim 9 \times 10^{19}$		$\sim 3 \times 10^{20}$	Arimoto et al. (1996)
$\sim (2.4 - 7.2) \times 10^{19}$	$\sim 3 \times 10^{20}$		Oka et al. (1998)
$\sim (2 - 4) \times 10^{19}$		$\sim 1.5 \times 10^{20}$	Strong et al. (2004)

The use of the standard virial mass as a tracer of the actual mass of molecular clouds was called into question by Oka et al. (1998), who argued that molecular clouds near the GC are not gravitationally bound, but instead confined by the high external pressure from hot gas and magnetic fields. Using the correct expression for the virial mass of pressure-confined clouds, they recalibrated the CO-luminosity–virial-mass relation for GC molecular clouds, whereupon they obtained $X_{\text{CO}} \sim 2.4 \times 10^{19} \text{ cm}^{-2} \text{K}^{-1} \text{km}^{-1} \text{s}$ near the GC. This value of X_{CO} is one order of magnitude lower than the value $X_{\text{CO}} \sim 3 \times 10^{20} \text{ cm}^{-2} \text{K}^{-1} \text{km}^{-1} \text{s}$ applying to gravitationally-bound molecular clouds in the Galactic disk. With their new value of X_{CO} , Oka et al. (1998) estimated the H_2 mass inside $r \simeq 375 \text{ pc}$ at $\sim 2 \times 10^7 M_\odot$. However, they pointed out that their derived values were lower limits, which could underestimate the true conversion factor and H_2 mass near the GC by up to a factor of 3.

More recently, Strong et al. (2004) showed that an outward radial gradient in X_{CO} was required to reconcile the predictions of their cosmic-ray propagation code GALPROP with the γ -ray profiles measured by EGRET/COMPTON, when they adopted the molecular and atomic gas distributions inferred from CO and HI surveys and assumed that the distribution of cosmic-ray sources follows the observed distribution of pulsars. They did not attempt to derive the precise r -dependence of X_{CO} implied by the measured γ -ray profiles, but they showed that a good fit to the EGRET data could be obtained with X_{CO} dropping from $\sim 1.5 \times 10^{20} \text{ cm}^{-2} \text{K}^{-1} \text{km}^{-1} \text{s}$ at $r = r_\odot$ to $\sim 4 \times 10^{19} \text{ cm}^{-2} \text{K}^{-1} \text{km}^{-1} \text{s}$ at $r = 2 \text{ kpc}$. Extrapolating their curve $X_{\text{CO}}(r)$ in to the origin yields $X_{\text{CO}} \sim (2 - 4) \times 10^{19} \text{ cm}^{-2} \text{K}^{-1} \text{km}^{-1} \text{s}$ at $r \rightarrow 0$ (see their Figure 2).

All the above estimates of the ^{12}CO -to- H_2 conversion factor are summarized in Table 2. It is clear that the value of X_{CO} near the GC remains fairly uncertain. More importantly, the very notion that N_{H_2} is proportional to $W_{^{12}\text{CO}}$ may be questionable (e.g., Dahmen et al. 1998). Nevertheless, the fact that three completely different methods to determine X_{CO} near the GC (far-infrared emission from dust, virial masses of molecular clouds and γ -ray emission from cosmic rays) broadly converge to a common range of values lends some credence to the presumed proportionality between N_{H_2} and $W_{^{12}\text{CO}}$. For the following, we adopt $X_{\text{CO}}(r \sim 0) = 5 \times 10^{19} \text{ cm}^{-2} \text{K}^{-1} \text{km}^{-1} \text{s}$ as a reference value, which we consider uncertain by a factor ~ 2 .

Once the value of X_{CO} is known, the H_2 spatial distribution can in principle be inferred from CO emission measurements. The overall disposition of CO emission in the Galaxy was brought to light by the early large-scale Galactic CO surveys, which revealed a sharp peak inside a few 100 pc from the GC, a deep depression between $\sim 1.5 \text{ kpc}$ and 3 kpc and a ring of enhanced emission (now designated the

Galactic disk molecular ring) between $\sim 3.5 \text{ kpc}$ and 6 kpc (see Combes 1991 for a review).

Sanders et al. (1984) presented a full-coverage Galactic ^{12}CO ($J = 1 \rightarrow 0$) survey, on the basis of which they constructed an axisymmetric model of the H_2 distribution in the Galaxy. According to their model (rescaled to $r_\odot = 8.5 \text{ kpc}$), molecular gas in the GB is confined to a disk with radius $\sim 1.3 \text{ kpc}$ and nearly constant thickness $\sim 70 \text{ pc}$, seen edge-on from the Sun and tilted counter-clockwise by $\sim 7^\circ$ with respect to the Galactic plane³ (so that its midplane passes from negative latitudes in the first quadrant to positive latitudes in the fourth quadrant). This tilted disk is prolonged by a rarefied molecular layer with approximately the same thickness, which smoothly joins up with the Galactic disk molecular ring. Taking a constant conversion factor $X_{\text{CO}} = 3.6 \times 10^{20} \text{ cm}^{-2} \text{K}^{-1} \text{km}^{-1} \text{s}$ for the whole Galaxy, Sanders et al. (1984) found that the H_2 space-averaged density could be approximated by

$$\langle n_{\text{H}_2} \rangle(\mathbf{r}) = \langle n_{\text{H}_2} \rangle_0(r) \exp \left[-\frac{1}{2} \left(\frac{z - z_0(r, \theta)}{H} \right)^2 \right], \quad (4)$$

where (after rescaling to $r_\odot = 8.5 \text{ kpc}$) $H \simeq (70 \text{ pc})/(2\sqrt{2 \ln 2}) \simeq 30 \text{ pc}$ out to $r \simeq 3 \text{ kpc}$, $z_0(r, \theta)$ is the local Galactic height of the H_2 midplane (given by the tilted disk geometry inside 1.3 kpc) and $\langle n_{\text{H}_2} \rangle_0(r)$ is the H_2 space-averaged density at z_0 , such that $\langle n_{\text{H}_2} \rangle_0(0 \rightarrow 450 \text{ pc}) \simeq 74 \text{ cm}^{-3}$, $\langle n_{\text{H}_2} \rangle_0(450 \text{ pc} \rightarrow 1.3 \text{ kpc}) \simeq 12 \text{ cm}^{-3}$ and $\langle n_{\text{H}_2} \rangle_0(1.3 \rightarrow 3 \text{ kpc}) \simeq 1.1 \text{ cm}^{-3}$. The corresponding H_2 masses inside $r = 450 \text{ pc}$, between 450 pc and 1.3 kpc , and in the depression zone between 1.3 kpc and 3 kpc are listed in Table 3.

Burton & Liszt (1992) presented higher-resolution ^{12}CO ($J = 1 \rightarrow 0$) observations toward the GC and pointed out that the central parts of the gaseous GB disk are in fact closely aligned with the Galactic plane. More specifically, they showed that the observed (l, b, v) pattern of ^{12}CO emission in the GB could be understood in the framework of a tilted and warped H_2 disk model with the following characteristics (rescaled to $r_\odot = 8.5 \text{ kpc}$): Out to $r \simeq 170 \text{ pc}$, the H_2 disk is flat, parallel to the Galactic plane and $\simeq 30 \text{ pc}$ thick (Gaussian scale height $\simeq 13 \text{ pc}$). Between $\simeq 170 \text{ pc}$ and 1.5 kpc , the H_2 disk flares linearly to a thickness $\simeq 300 \text{ pc}$ (uncertain value), and this flaring is accompanied by a warp such that the H_2 midplane becomes tilted with respect to the Galactic plane, by an angle that varies sinusoidally with Galactic azimuth between -13° at $\theta = 45^\circ$ (so that $b < 0^\circ$ in the near, first-quadrant sector) and $+13^\circ$ at $\theta = 225^\circ$ ($b > 0^\circ$ in the far, fourth-quadrant sector) (see their Figure 5). Overall, the warped

³ Here, and in the rest of the paper, the Galactic plane is defined as the plane $b = 0^\circ$, which is slightly different from the plane of the solar circle.

Table 3. Estimated values of the mass of interstellar H₂ in specific regions of the GB.

Region of space	Radial range	H ₂ mass	Reference
Tilted GB disk : inner part	0 – 450 pc	$\sim 1.75 \times 10^8 M_\odot$	Sanders et al. (1984)
outer part	450 pc – 1.3 kpc	$\sim 2.1 \times 10^8 M_\odot$	"
Depression zone	1.3 – 3 kpc	$\sim 9 \times 10^7 M_\odot$	"
GC molecular disk	$\simeq 0 - 150$ pc	$\sim 2.4 \times 10^7 M_\odot$	Sofue (1995a)
"Expanding molecular ring"	straddling $r \simeq 180$ pc	$\sim 5 \times 10^6 M_\odot$	Sofue (1995b)
GB region $-1.5^\circ \leq l \leq 3.5^\circ$	$\simeq 0 - 375$ pc (off-centered)	$\sim (2 - 6) \times 10^7 M_\odot$	Sodroski et al. (1995)
GB region $ l \leq 2.5^\circ$	$\simeq 0 - 375$ pc	$\sim (2 - 6) \times 10^7 M_\odot$	Oka et al. (1998)
Nuclear bulge	$\simeq 0 - 280$ pc (off-centered)	Dense gas : $\sim (1.2 - 6.4) \times 10^7 M_\odot$ Thin gas : $\sim (0.7 - 1.4) \times 10^7 M_\odot$	Dahmen et al. (1998) "

H₂ disk appears tilted out of the Galactic plane and inclined to the line of sight, very much like the tilted H I disk of Burton & Liszt (1978) (see section 2.3). The warped H₂ disk also bears a resemblance to Sanders et al.'s (1984) tilted H₂ disk, but it differs by its substantial flaring and by the direction of maximum tilt ($\theta = 45^\circ - 225^\circ$, as opposed to $\theta = 90^\circ - 270^\circ$ in Sanders et al.). Interestingly, the H₂ space-averaged density in the warped disk can be expressed by Equation 4, with $H \simeq 13$ pc inside $r \simeq 170$ pc and $H \simeq 0.088$ ($r - 22$ pc) between $\simeq 170$ pc and 1.5 kpc, and with $\langle n_{\text{H}_2} \rangle_0 \propto 1/H$ (such that the H₂ column density through the disk has a constant, albeit unspecified, value). Besides its geometric parameters, the warped H₂ disk model also possesses two kinematic parameters describing rotation and expansion motions, respectively.

Let us now focus on the innermost Galactic regions, inside a few 100 pc from the GC, where molecular gas tends to concentrate. Sofue (1995a) investigated the H₂ morphology and kinematics inside $|l| \simeq 1^\circ$ ($r_\perp \simeq 150$ pc), based on the AT&T Bell Laboratories survey of ¹³CO ($J = 1 \rightarrow 0$) emission conducted by Bally et al. (1987). He adopted $X_{\text{CO}} = 9.2 \times 10^{19} \text{ cm}^{-2} \text{ K}^{-1} \text{ km}^{-1} \text{ s}$ (from a slightly modified version of Equation 3) together with $W_{12\text{CO}}/W_{13\text{CO}} = 6.2$ (measured intensity ratio averaged over $|l| \lesssim 20^\circ$). The most salient continuous features in the longitude-velocity (l, v) diagrams of the GC molecular disk are two apparently rigidly-rotating ridges. Sofue (1995a) interpreted these ridges as the (l, v) traces of two dense material arms, which together would form a rotating ring with mean radius $\simeq 120$ pc and vertical thickness ~ 15 pc (except for the massive molecular complexes around Sgr B and C, whose thickness reaches $\sim 30 - 60$ pc). An analysis of the velocity-integrated intensity maps yields a total H₂ mass $\sim 2.4 \times 10^7 M_\odot$ for the disk, with $\sim 1.1 \times 10^7 M_\odot$ in Arm I and $\sim 0.8 \times 10^7 M_\odot$ in Arm II, and an H₂ mass $\sim 2.8 \times 10^7 M_\odot$ for the entire region $r_\perp \lesssim 150$ pc. By examining a somewhat wider section of Bally et al.'s (1987) survey, Sofue (1995b) estimated that the "expanding molecular ring" that surrounds the GC molecular disk has a mean radius $\simeq 180$ pc (as already established before), a radial thickness ~ 15 pc, a vertical thickness ~ 100 pc and an H₂ mass $\sim 5 \times 10^6 M_\odot$ (80% of which belongs to the region $r_\perp \lesssim 150$ pc).

Dahmen et al. (1998) gained additional information on the spatial structure and physical state of molecular gas near the GC by analyzing a SMWT C¹⁸O ($J = 1 \rightarrow 0$) survey of the central region $-1.05^\circ \leq l \leq 3.6^\circ$, in conjunction with the SMWT ¹²CO ($J = 1 \rightarrow 0$) survey of the broader region $-12^\circ \leq l \leq 13^\circ$ presented by Bitran et

al. (1997). For both isotopomers,⁴ they performed radiative transfer calculations in the Large Velocity Gradient (LVG) approximation, and they adopted abundance ratios $^{12}\text{CO}/\text{H}_2 = 10^{-4}$ and $\text{C}^{18}\text{O}/\text{H}_2 = 4 \times 10^{-7}$. Their calculations enabled them to estimate the kinetic temperature, volume density and total mass of molecular gas in the nuclear bulge, which they assumed to extend over the longitude range $-1.5^\circ \leq l \leq 2.25^\circ$ (projected half-size $\simeq 280$ pc). They found that most of the C¹⁸O emission is likely to originate in molecular gas with kinetic temperature $T \sim 50$ K and H₂ density $n_{\text{H}_2} \sim 10^{3.5} \text{ cm}^{-3}$, and they argued that the associated H₂ mass in the nuclear bulge is comprised between $\sim 1.2 \times 10^7 M_\odot$ and $6.4 \times 10^7 M_\odot$. Furthermore, they noted significant differences between the C¹⁸O and ¹²CO intensity maps, which they interpreted as evidence for the presence of a widespread, high-temperature and low-density gas component, detected in ¹²CO but not in C¹⁸O. This thin gas would have $T \sim 150$ K, $n_{\text{H}_2} \sim 10^{2.5} \text{ cm}^{-3}$ and an H₂ mass in the nuclear bulge between $\sim 0.7 \times 10^7 M_\odot$ and twice that value.

Another powerful method to probe the physical conditions in molecular gas near the GC is to compare emission lines from different J levels of ¹²CO. In this spirit, Oka et al. (1998) mapped the region $|l| \leq 2.5^\circ$ in ¹²CO ($J = 2 \rightarrow 1$) emission with the NRO survey telescope, and they resorted to previous ¹²CO ($J = 1 \rightarrow 0$) maps from Bitran (1987) for comparison. Their analysis of the ¹²CO ($J = 2 \rightarrow 1$) / ¹²CO ($J = 1 \rightarrow 0$) intensity ratio indicates that the CO luminosity of the innermost ~ 400 pc is dominated by emission from low-density gas with $n_{\text{H}_2} \sim 10^{2.5} \text{ cm}^{-3}$. To reconcile this finding with the inference from CS, NH₃ and HCN observations that high-density gas with $n_{\text{H}_2} \gtrsim 10^4 \text{ cm}^{-3}$ prevails, Oka et al. (1998) advanced the view that molecular gas actually exists in two distinct components: a low-density ($n_{\text{H}_2} \lesssim 10^3 \text{ cm}^{-3}$) component present in "diffuse" clouds with a large filling factor, and a high-density ($n_{\text{H}_2} \gtrsim 10^4 \text{ cm}^{-3}$) component present in "clumps" with a small filling factor. This view of a two-component molecular gas in the GC region has found support in several subsequent studies relying on other tracer molecules (e.g., Rodríguez-Fernández et al. 2001; Oka et al. 2005; Magnani et al. 2006). Let us simply mention that the warm ($T \sim 150$ K), and presumably low-density, component detected by Rodríguez-Fernández et al. (2001) would on average represent $\sim 30\%$ of the total molecular gas.

⁴ Isomers having the same number of isotopically distinct atoms but differing in the positions of these atoms. The term "isotopomer" results from the contraction of the words "isotope" and "isomer".

Table 4. Estimated values of the mass of interstellar H_2 in specific regions of the GB, deduced from ^{12}CO measurements (or from ^{13}CO measurements combined with an assumed ^{12}CO -to- ^{13}CO intensity ratio) together with $X_{\text{CO}} = 5 \times 10^{19} \text{ cm}^{-2} \text{ K}^{-1} \text{ km}^{-1} \text{ s}$.

Region of space	Radial range	H_2 mass	Original reference ^a
Tilted GB disk : inner part	0 – 450 pc	$\sim 2.4 \times 10^7 M_\odot$	Sanders et al. (1984)
outer part	450 pc – 1.3 kpc	$\sim 2.9 \times 10^7 M_\odot$	"
Depression zone	1.3 – 3 kpc	$\sim 1.3 \times 10^7 M_\odot$	"
GC molecular disk	$\simeq 0 - 150 \text{ pc}$	$\sim 1.3 \times 10^7 M_\odot$	Sofue (1995a)
“Expanding molecular ring”	straddling $r \simeq 180 \text{ pc}$	$\sim 2.7 \times 10^6 M_\odot$	Sofue (1995b)
GB region $-1^\circ 5 \leq l \leq 3^\circ 5$	$\simeq 0 - 375 \text{ pc}$ (off-centered)	$\sim 4.4 \times 10^7 M_\odot$	Sodroski et al. (1995)
GB region $ l \leq 2^\circ 5$	$\simeq 0 - 375 \text{ pc}$	$\sim 4.2 \times 10^7 M_\odot$	Oka et al. (1998)

^a Reference for the corresponding mass estimate given in Table 3, which we rescaled to our adopted value of X_{CO} .

Higher- J transitions of ^{12}CO also provide a valuable diagnostic tool for molecular gas. For instance, Martin et al. (2004) surveyed the region $-1^\circ 3 \leq l \leq 2^\circ$ in ^{12}CO ($J = 4 \rightarrow 3$) and ^{12}CO ($J = 7 \rightarrow 6$) emission with the AST/RO telescope, and they analyzed their ^{12}CO ($J = 4 \rightarrow 3$) and ^{12}CO ($J = 7 \rightarrow 6$) maps together with existing ^{12}CO ($J = 1 \rightarrow 0$) and ^{13}CO ($J = 1 \rightarrow 0$) maps from Stark et al. (1988) and Bally et al. (1987, 1988). Like Dahmen et al. (1998), they worked with the LVG approximation and they took $^{12}\text{CO}/\text{H}_2 = 10^{-4}$. What emerges from their study is that the molecular gas kinetic temperature decreases from $T \gtrsim 70 \text{ K}$ at the edges of cloud complexes to $T \lesssim 50 \text{ K}$ in their interiors, and that the H_2 density spans the validity range of their LVG analysis ($\sim 10^{2.5} - 10^{4.5} \text{ cm}^{-3}$), with typical values $n_{\text{H}_2} \sim 10^{3.5} \text{ cm}^{-3}$ inside cloud complexes.

Finally, Sawada et al. (2004) devised a purely observational method to deconvolve sky maps of CO emission into a face-on view of the molecular gas distribution near the GC, based on a quantitative comparison between the 2.6-mm ^{12}CO emission line and the 18-cm OH absorption line. Their face-on map exhibits a strong central condensation (corresponding to the CMZ), which is elongated along an axis inclined by $\sim 70^\circ$ to the line of sight (so that its near end lies at positive longitudes), $\sim 500 \text{ pc} \times 200 \text{ pc}$ in size, and possibly composed of a pair of arms (as suggested by Sofue 1995a). The so-called “expanding molecular ring” lies at the periphery of the central condensation, without clearly separating from it. It, too, is elongated and inclined (by an uncertain angle $< 70^\circ$) toward positive longitudes, though it does not actually stand out as a coherent entity in the face-on map. Instead, Sawada et al.’s (2004) results tend to substantiate the idea that the “expanding molecular ring” arises from the projection of interstellar gas moving along highly elongated orbits in response to the gravitational potential of the Galactic bar (see section 3 for further details).

Table 3 provides a summary of all the H_2 masses estimated in this subsection. Clearly, the H_2 mass derived by Sanders et al. (1984) for the innermost region is significantly greater than the other estimates. This is only because these authors used a much larger value of the conversion factor, X_{CO} , more typical of the Galactic disk at large. If we now rescale all the H_2 masses deduced from ^{12}CO measurements (or from ^{13}CO measurements combined with an assumed ^{12}CO -to- ^{13}CO intensity ratio) in Table 3 to our adopted reference value $X_{\text{CO}} = 5 \times 10^{19} \text{ cm}^{-2} \text{ K}^{-1} \text{ km}^{-1} \text{ s}$, we obtain the H_2 masses listed in Table 4. These masses agree with each other to within a factor of ~ 2 . Moreover, they grossly match the total hydrogen masses inferred from in-

frared dust measurements by Launhardt et al. (2002) (see Table 1), consistent with the notion that most of the interstellar gas in the CMZ is in molecular form.

2.3. Atomic gas

Virtually all our observational knowledge on the interstellar atomic gas near the GC stems from spectral studies of the HI 21-cm line in emission or in absorption. The early NRAO surveys of HI 21-cm emission over the longitude range $-11^\circ \leq l \leq 13^\circ$ led Burton & Liszt (1978) and Liszt & Burton (1980) to propose a tilted disk model for the HI spatial distribution inside $r \sim 2 \text{ kpc}$. The model parameters were determined iteratively by generating synthetic 21-cm emission spectra and adjusting them to the observed spectra.

In Burton & Liszt’s (1978) model (rescaled to $r_\odot = 8.5 \text{ kpc}$), the HI disk is axisymmetric, 1.3 kpc in radius, 200 pc thick (Gaussian scale height of 85 pc), tilted by 22° out of the Galactic plane (with the first/fourth quadrant side at negative/positive latitudes) and inclined by 78° to the plane of the sky (with the near/far side at negative/positive latitudes), such that the normal to the HI disk forms a 25° angle with the z -axis. The HI space-averaged density in the disk is given by a Gaussian function of distance to the HI midplane, z_d ,

$$\langle n_{\text{HI}} \rangle(z_d) = (0.39 \text{ cm}^{-3}) \exp \left[-\frac{1}{2} \left(\frac{z_d}{85 \text{ pc}} \right)^2 \right], \quad (5)$$

which implies a total HI mass in the disk $\simeq 1.1 \times 10^7 M_\odot$. Finally, the HI gas within the disk has rotation and expansion motions of comparable magnitudes.

Liszt & Burton (1980) argued that the observed kinematics of the HI gas could be more plausibly explained by a tilted elliptical disk model, in which the gas moves along closed elliptical orbits. Thus, in Liszt & Burton’s (1980) model (again rescaled to $r_\odot = 8.5 \text{ kpc}$), the HI disk is elliptical, with semi-major axis 1.6 kpc and axis ratio 3.1 : 1. Its thickness remains 200 pc, but the tilt and inclination angles are now $13^\circ 5$ to the Galactic plane and 70° to the plane of the sky (entailing a 24° angle between the disk normal and the z -axis), and the major axis is oriented at $48^\circ 5$ clockwise to the “inclined x -axis” (corresponding to a $51^\circ 5$ angle to the line of sight) (see their Figure 1). The HI space-averaged density in the disk is still given by Equation 5, but the total HI mass in the disk now amounts to $\simeq 5.2 \times 10^6 M_\odot$.

A different modification to Burton & Liszt’s (1978) original model can be found in the paper by Burton & Liszt

Table 5. Estimated values of the mass of interstellar HI in specific regions of the GB.

Region of space	Radial range	HI mass	Reference
Tilted GB disk :			
Axisymmetric	0 – 1.3 kpc	$\sim 1.1 \times 10^7 M_\odot$	Burton & Liszt (1978)
Elliptical	0 – 1.6 kpc / 0 – 0.52 kpc	$\sim 5.2 \times 10^6 M_\odot$	Liszt & Burton (1980)
Axisymmetric	See Equation 6	$\sim 2.2 \times 10^6 M_\odot$	Burton & Liszt (1993)
Inner part of GB disk	$\sim 0 - 300$ pc (off-centered)	$\sim 2.3 \times 10^6 M_\odot$	Rohlfs & Braunsfurth (1982)
180-pc molecular ring	straddling $r \simeq 175$ pc (off-centered)	$\sim 8 \times 10^5 M_\odot$	"

(1993). There, the HI spatial distribution within the GB disk is modeled in a slightly more complicated manner, with a HI space-averaged density depending on both r and z_d :

$$\langle n_{\text{HI}} \rangle(r, z_d) = \left\{ (0.82 \text{ cm}^{-3}) \exp \left[- \left(\frac{r}{450 \text{ pc}} \right)^2 \right] + (0.10 \text{ cm}^{-3}) \exp \left[- \left(\frac{r}{800 \text{ pc}} \right)^2 \right] \right\} \times \exp \left[- \frac{1}{2} \left(\frac{z_d}{50 \text{ pc}} \right)^2 \right]. \quad (6)$$

The corresponding FWHM thickness is $\simeq 118$ pc and the total HI mass is $\simeq 2.2 \times 10^6 M_\odot$. However, the emphasis of the paper is placed on the kinematic aspects of atomic gas in the GB, and as the authors themselves recognize, Equation 6 may have little intrinsic significance. Therefore, we do not regard the associated mass estimate as particularly trustworthy.

Rohlfs & Braunsfurth (1982) presented a more refined description of the morphology and kinematics of atomic gas in the central parts of the HI GB disk. They analyzed 21-cm emission as well as absorption spectra obtained with the Effelsberg telescope at longitudes $|l| \leq 1^\circ 5$, and they made comparisons between both types of spectra in order to locate the major HI features relative to the GC. Like Burton & Liszt (1978), they started from the premise that the velocity field includes rotation and expansion. Furthermore, they used an axisymmetric rotation curve inferred from a Galactic mass model as an independent distance indicator, and they assumed that the major HI features are nearly circular (though not necessarily concentric with the GC). Because of these stringent assumptions, largely refuted by more recent work, too much reality should not be ascribed to the precise quantitative estimates provided by Rohlfs & Braunsfurth (1982). Nevertheless, a couple of important points deserve mentioning. First, although the HI GB disk as a whole is markedly tilted, its central parts are approximately parallel to the Galactic plane (as is the case for the warped H₂ disk of Burton & Liszt 1992; see section 2.2). Second, the 180-pc molecular ring is visible in 21-cm emission, without however being prominent. For reference, Rohlfs & Braunsfurth (1982) estimated that the inner part of the HI GB disk has a radius ~ 300 pc, a thickness ~ 90 pc and an HI mass $\sim 2.3 \times 10^6 M_\odot$, while the 180-pc molecular ring has a mean radius $\simeq 175$ pc, a vertical thickness ~ 60 pc and an HI mass $\sim 8 \times 10^5 M_\odot$.

Unfortunately, the atomic gas does not benefit from the wide variety of diagnostic spectral lines or from the vast number of high-resolution surveys as are presently available for the molecular gas. Further genuine progress in our understanding of interstellar atomic gas near the GC

will probably have to await the release of new data from the GC extension of the Southern Galactic Plane Survey (McClure-Griffiths, private communication). In the meantime, one should bear in mind that the spatial distribution and kinematics of the atomic gas might not be as drastically different from those of the molecular gas as traditionally believed. Liszt & Burton (1996) advanced several cogent arguments pointing to the congruence of both gases in position and in velocity, and they attributed their apparent disparities to differences in the observational conditions (angular resolution, sky coverage and signal-to-noise ratio) of HI *versus* CO, in the thin *versus* thick optical-depth regime and in the presence *versus* absence of absorption (see also Liszt & Burton 1978). In addition, they emphasized that the kinematic features appearing in the HI and CO spectra (notably the “expanding molecular ring”) do not correspond to discrete material bodies, but instead result from kinematic projection effects.

Again, we close up the subsection with a summary table (Table 5) including all our mass estimates. For completeness, we can add that the HI mass inside $r \simeq 300$ pc is $\simeq 5.8 \times 10^5 M_\odot$ in Burton & Liszt’s (1978) model and $\simeq 6.6 \times 10^5 M_\odot$ in their (1993) model, as opposed to $\sim 3.1 \times 10^6 M_\odot$ in Rohlfs & Braunsfurth (1982). Hence, there is roughly a factor of 5 discrepancy between Burton & Liszt on the one hand and Rohlfs & Braunsfurth on the other hand. The same factor exists, for the entire HI GB disk, between the old and new models of Burton & Liszt, but as we already mentioned earlier, the HI mass deduced from their 1993 model should not be taken too seriously. If we disregard this mass estimate, we may conclude from a comparison between Tables 4 and 5 that the HI mass of the entire GB disk represents but $\sim 10\% - 20\%$ of its H₂ mass.

2.4. Ionized gas

Radio signals from pulsars and other (Galactic and extragalactic) compact sources provide a unique source of information on the ionized component of the interstellar gas. Cordes & Lazio (2002) assembled all the useful data (dispersion measures, scattering measures and independent distance estimates) available at the end of 2001 to construct a new non-axisymmetric model of the spatial distribution of interstellar free electrons in the Galaxy. This “NE2001 model”, which incorporates separate multi-wavelength data on the spiral structure of the Galaxy, the local interstellar medium and the GC region, supersedes the earlier models of Cordes et al. (1991) and Taylor & Cordes (1993). It includes a smooth large-scale component, which consists of two axisymmetric disks and five spiral arms, a smooth GC component, a contribution from the local interstellar medium, and individual clumps and voids.

Retaining solely the smooth components present inside 3 kpc, we can write the free-electron space-averaged density in the GB as

$$\langle n_e \rangle(\mathbf{r}) = \langle n_e \rangle_1(r, z) + \langle n_e \rangle_2(r, z) + \langle n_e \rangle_3(r, z), \quad (7)$$

where

$$\begin{aligned} \langle n_e \rangle_1(r, z) = & (0.05 \text{ cm}^{-3}) \left[\cos \left(\pi \frac{r}{2L_1} \right) u(L_1 - r) \right] \\ & \times \text{sech}^2 \left(\frac{z}{H_1} \right), \end{aligned} \quad (8)$$

with $L_1 = 17$ kpc and $H_1 = 950$ pc, for the outer thick disk (u is the unit step function),

$$\begin{aligned} \langle n_e \rangle_2(r, z) = & (0.09 \text{ cm}^{-3}) \exp \left[- \left(\frac{r - L_2}{L_2/2} \right)^2 \right] \\ & \times \text{sech}^2 \left(\frac{z}{H_2} \right), \end{aligned} \quad (9)$$

with $L_2 = 3.7$ kpc and $H_2 = 140$ pc, for the inner thin disk⁵, and

$$\begin{aligned} \langle n_e \rangle_3(r, z) = & (10 \text{ cm}^{-3}) \exp \left[- \frac{x^2 + (y - y_3)^2}{L_3^2} \right] \\ & \times \exp \left[- \frac{(z - z_3)^2}{H_3^2} \right], \end{aligned} \quad (10)$$

with $y_3 = -10$ pc, $z_3 = -20$ pc, $L_3 = 145$ pc and $H_3 = 26$ pc, for the GC component.⁶ Strictly speaking, the offset ellipsoid exponential in Equation 10 should be truncated to zero for arguments smaller than -1 . However, such a discontinuity was introduced into the model to reflect the abrupt changes observed in the distribution of scattering diameters for OH masers in the GC rather than an abrupt drop-off in the free-electron density. Since we are interested only in the free-electron density (as opposed to both the density and its fluctuations), we are entitled to relax the constraint arising from scattering diameters and omit to truncate the ellipsoid exponential in Equation 10 (Lazio, private communication). Then the GC component remains dominant near the midplane out to $r \simeq 335$ pc. The rest of the GB is largely dominated by the thick disk, except for a narrow wedge starting at $(r, z) \simeq (2.3 \text{ kpc}, 0)$ and opening outward, wherein the thin disk takes over.

To convert the above free-electron density into an ionized-hydrogen density, we follow conventional wisdom and assume that the molecular and atomic media (discussed in sections 2.2 and 2.3, respectively) can be considered as completely neutral, while the ionized medium can be divided into a warm ionized medium (WIM), where hydrogen is entirely ionized and helium completely neutral, and a hot ionized medium (HIM), where hydrogen and helium are both fully ionized. If we further denote by f_{HIM} the fraction of ionized gas belonging to the HIM and remember that helium represents 10% by number of hydrogen (see beginning of section 2), we find that the ionized-hydrogen

space-averaged density is related to the free-electron space-averaged density through

$$\langle n_{\text{H}^+} \rangle = \frac{1}{1 + 0.2 f_{\text{HIM}}} \langle n_e \rangle. \quad (11)$$

The HIM fraction, f_{HIM} , is quite uncertain, but fortunately, its exact value has little impact on the inferred H^+ density, $\langle n_{\text{H}^+} \rangle$, which varies between $\langle n_e \rangle$ if $f_{\text{HIM}} = 0$ and $0.83 \langle n_e \rangle$ if $f_{\text{HIM}} = 1$.

The total H^+ mass in the interstellar GB and the contributions from the thick disk, thin disk and GC component are obtained by integrating Equations 8, 9 and 10, divided by the factor $(1 + 0.2 f_{\text{HIM}})$, out to $r = 3$ kpc. For reference, if $f_{\text{HIM}} = 0$, the thick disk has an H^+ mass of $6.4 \times 10^7 M_\odot$ inside 3 kpc, with $1.8 \times 10^6 M_\odot$ inside 500 pc and $1.6 \times 10^5 M_\odot$ inside 150 pc; the thin disk has an H^+ mass of $8.3 \times 10^6 M_\odot$ inside 3 kpc, with $1.8 \times 10^4 M_\odot$ inside 500 pc and $1.0 \times 10^3 M_\odot$ inside 150 pc; and the GC component has a total H^+ mass of $7.5 \times 10^5 M_\odot$, with $5.0 \times 10^5 M_\odot$ inside 150 pc and negligible amounts outside 500 pc. The resulting total H^+ masses inside 150 pc, 500 pc and 3 kpc are displayed in Table 6. A comparison with our previous tables (Table 1 or Table 4 with an assumed H I -to- H_2 mass ratio $\sim 10\% - 20\%$) suggests that ionized gas accounts for only $\sim 4\% - 5\%$ of the total interstellar gas in the region $r \lesssim 150$ pc, $\sim 4\% - 8\%$ in the region $r \lesssim 500$ pc, and $\sim 30\% - 50\%$ on average over the entire GB ($r \lesssim 3$ kpc). Not surprisingly, the fraction of ionized gas increases not only with $|z|$ (as indicated by the comparatively large scale height in Equation 8), but also with r .

Lazio and Cordes (1998) discussed the nature of the medium responsible for the observed scattering. They proposed that scattering arises in thin layers on the surfaces of molecular clouds. These layers would either be the photoionized skins of molecular clouds, with $T_e \sim 10^4$ K and $n_e \gtrsim 10^3 \text{ cm}^{-3}$, or the interfaces between molecular clouds and the hot ($\sim 10^7$ K) ambient gas, with $T_e \sim (10^5 - 10^6)$ K and $n_e \sim (5 - 50) \text{ cm}^{-3}$. In both cases, the scattering medium would have a small filling factor. However, the scattering medium possibly constitutes but a small part of the ionized medium; therefore, its morphology and physical parameters are not necessarily representative of the ionized medium in general.

The best source of information on the morphology and physical parameters of the warm component of the ionized medium near the GC comes from the thermal (free-free) component of the radio continuum emission and from radio recombination lines. In general, thermal continuum measurements are used to image the ionized gas and to estimate its electron density and temperature, while recombination line measurements make it possible to investigate the kinematics of the ionized gas and also to estimate its electron temperature.

As explained in the review by Mezger & Pauls (1979), the thermal radio continuum emission is produced in an extended ionized medium (here referred to as the WIM) and in individual HII regions. On the sky, the thermal radio emission appears closely correlated with far-infrared dust emission, and less well correlated with CO emission, which is asymmetric (see section 2.2), more extended in longitude and less extended in latitude. To quote Mezger & Pauls (1979), “this suggests that the [WIM] may be ionization bounded along the Galactic plane, but density

⁵ The expression of $g_2(r)$ given in Table 2 of Cordes & Lazio (2002) contains a typo: A_a should be A_2 in the numerator and $A_2/2$ in the denominator (Lazio, private communication).

⁶ The (x, y, z) coordinates used by Cordes & Lazio (2002) correspond to (y, x, z) in our coordinate system (see Figure 1).

Table 6. Estimated values of the mass of interstellar H^+ (total mass or partial contribution from the WIM or HIM/VHIM) in specific regions of the GB. The total H^+ masses deduced from the NE2001 model for the free-electron density (Cordes & Lazio 2002) are those obtained under the extreme assumption that 100% of the ionized medium is warm (so that $\langle n_{H^+} \rangle = \langle n_e \rangle$). If, in reality, a fraction f_{HIM} of the ionized medium is hot, these masses should be divided by the factor $(1 + 0.2 f_{HIM})$ (see Equation 11).

Region of space	Radial range	H^+ mass			Reference
		Total	WIM	HIM/VHIM	
Galactic bulge : innermost	0 – 150 pc	$\sim 6.6 \times 10^5 M_\odot$			Cordes & Lazio (2002)
intermediate	0 – 500 pc	$\sim 2.6 \times 10^6 M_\odot$			"
total	0 – 3 kpc	$\sim 7.3 \times 10^7 M_\odot$			"
Smaller ellipsoid	$\simeq 0 - 47$ pc		$\sim 1.2 \times 10^5 M_\odot$		Mezger & Pauls (1979)
Larger ellipsoid	$\simeq 0 - 112$ pc		$\sim 4.7 \times 10^5 M_\odot$		"
Galactic bulge	0 – 3 kpc			$\sim 8 \times 10^6 M_\odot$	Snowden et al. (1997)
				$\sim 1.2 \times 10^7 M_\odot$	Almy et al. (2000)
10-keV plasma : innermost	0 – 150 pc			$\sim 5.5 \times 10^4 M_\odot$	{ Yamauchi et al. (1990)
					{ Koyama et al. (1996)
total	$\sim 0 - 250$ pc			$\sim 9.5 \times 10^4 M_\odot$	"

bounded perpendicular to it.” As a first rough approximation, Mezger & Pauls (1979) modeled the WIM by the superposition of two oblate ellipsoids with the following characteristics⁷ (rescaled to $r_\odot = 8.5$ kpc): the larger ellipsoid is $\simeq (225 \text{ pc})^2 \times 90$ pc in size and has $T_e \simeq 5000$ K, $n_e \simeq 8 \text{ cm}^{-3}$ and $M_{H^+} \simeq 4.7 \times 10^5 M_\odot$, while the smaller ellipsoid is $\simeq (95 \text{ pc})^2 \times 55$ pc in size and has $T_e \simeq 5000$ K, $n_e \simeq 18 \text{ cm}^{-3}$ and $M_{H^+} \simeq 1.2 \times 10^5 M_\odot$ (see Table 6). Altogether, the central electron density is $\simeq 26 \text{ cm}^{-3}$ and the total H^+ mass is $\simeq 5.9 \times 10^5 M_\odot$. For comparison, in the NE2001 model of Cordes & Lazio (2002), the GC component has an ellipsoid exponential distribution with FWHM size $\simeq (241 \text{ pc})^2 \times 43$ pc (comparable in radial extent, but significantly more oblate than the larger ellipsoid of Mezger & Pauls 1979), a central electron density of 10 cm^{-3} and a total H^+ mass of $(7.5 \times 10^5 M_\odot)/(1 + 0.2 f_{HIM})$. Evidently, the good agreement found for the H^+ masses is a little fortuitous.

A number of studies on the WIM near the GC have been carried out since the review of Mezger & Pauls (1979). For instance, Mehringer et al. (1992, 1993) observed the Sgr B region with the VLA, both at several wavelengths in the radio continuum and in the $H_{110\alpha}$ radio recombination line. They estimated the r.m.s. electron density outside compact HII regions at $\sim 80 \text{ cm}^{-3}$ in Sgr B1 and $\sim 60 \text{ cm}^{-3}$ in Sgr B2.

Besides the WIM, the ionized medium near the GC contains a hot component (referred to as the HIM) which can be detected through its X-ray thermal emission. Maps of the diffuse X-ray background in the $(0.5 - 2.0)$ keV energy band from the ROSAT all-sky survey reveal an extended zone of enhanced emission in the general direction of the GC (Snowden et al. 1997). Although part of the enhancement can be attributed to the nearby Loop I SB, Snowden et al. (1997) argued, based on the latitude profile of the excess emission, on the absorption trough running along the

Galactic plane and on the deep shadows cast by relatively distant molecular clouds, that the bulk of the enhancement arises from a bulge of hot, X-ray emitting gas around the GC. They went on to propose a crude model for the X-ray bulge, which relies on the $(0.5 - 2.0)$ keV ROSAT data corrected for foreground absorption by interstellar $H\text{I}$ and H_2 , and which assumes that the X-ray emitting gas is in collisional ionization equilibrium. In their model, the hot gas has a temperature of 4×10^6 K, an electron space-averaged density (again rescaled to $r_\odot = 8.5$ kpc)

$$\langle n_e \rangle_{HIM}(r, z) = (0.0034 \text{ cm}^{-3}) u(6 \text{ kpc} - r) \times \exp \left[- \left(\frac{|z|}{2 \text{ kpc}} \right) \right], \quad (12)$$

and hence an H^+ mass $\simeq 8 \times 10^6 M_\odot$ inside $r = 3$ kpc.

As follow-up work, Almy et al. (2000) analyzed the shadows cast by a distant molecular cloud complex against the X-ray enhancement in the $\frac{3}{4}$ keV and 1.5 keV ROSAT bands, and came to the conclusion that a significant fraction of the observed radiation in that direction is indeed emitted beyond the cloud complex, most likely in an X-ray bulge surrounding the GC. They also derived a simple, albeit more realistic, model for the X-ray bulge, in which the X-ray emitting gas is an adiabatic polytrope ($P \propto \rho^{5/3}$) in hydrostatic balance (in the Galactic gravitational potential of Wolfire et al. 1995). Like Snowden et al. (1997), they assumed collisional ionization equilibrium and they accounted for foreground absorption. They found that the best fit to the $\frac{3}{4}$ keV ROSAT data is reached for a central gas temperature of 8.2×10^6 K and a central electron density of 0.011 cm^{-3} .

Almy et al. (2000) provided no analytical expressions to describe the spatial variation of the hot gas parameters. Nonetheless, all the useful expressions can be retrieved by solving the hydrostatic equation, $-\nabla P - \rho \nabla \phi = 0$, together with the polytropic assumption, $P = K \rho^{5/3}$, and Wolfire et al.’s (1995) representation of the Galactic gravitational

⁷ In the rest of this section, all density estimates deduced from emission measures implicitly assume that the phase under consideration occupies all the interstellar volume. If the considered phase actually has a volume filling factor ϕ , each of our density estimates corresponds in fact to the geometric mean between the true and space-averaged densities, and the actual true/space-averaged density is obtained by dividing/multiplying our density estimate by $\sqrt{\phi}$.

potential,

$$\phi(r, z) = -(225 \text{ km s}^{-1})^2 \times \left\{ \frac{C_1}{\sqrt{r^2 + (a_1 + \sqrt{z^2 + b_1^2})^2}} + \frac{C_2}{a_2 + \sqrt{r^2 + z^2}} - C_3 \ln \frac{\sqrt{1 + \frac{a_3^2 + r^2 + z^2}{r_h^2}} - 1}{\sqrt{1 + \frac{a_3^2 + r^2 + z^2}{r_h^2}} + 1} \right\}, \quad (13)$$

where $C_1 = 8.887 \text{ kpc}$, $a_1 = 6.5 \text{ kpc}$, $b_1 = 0.26 \text{ kpc}$, $C_2 = 3.0 \text{ kpc}$, $a_2 = 0.70 \text{ kpc}$, $C_3 = 0.325$, $a_3 = 12 \text{ kpc}$ and $r_h = 210 \text{ kpc}$. In this manner, it is found that the electron space-averaged density of the HIM can be written in the form

$$\langle n_e \rangle_{\text{HIM}}(r, z) = \left\{ (0.011 \text{ cm}^{-3})^{2/3} - (1.73 \times 10^{-17} \text{ cm}^{-4} \text{ s}^2) \times [\phi(r, z) - \phi(0, 0)] \right\}^{1.5} \quad (14)$$

and that the H^+ mass inside $r = 3 \text{ kpc}$ (with $|z| \leq 5 \text{ kpc}$) amounts to $\simeq 1.2 \times 10^7 M_\odot$.

Hence, the mass of hot H^+ predicted by Almy et al.'s (2000) model for the region $r \leq 3 \text{ kpc}$ is 1.5 times that predicted by Snowden et al.'s (1997) cruder model. In view of Table 6 and the discussion below Equation 11, Almy et al.'s model suggests that hot gas globally represents $\sim 17\%$ of all the ionized gas, and thus $\sim 5\% - 8.5\%$ of the total interstellar gas, in the GB. However, little can be said about the spatial variation of the hot gas fraction, because the assumption of an adiabatic polytrope in hydrostatic balance is made for modeling convenience rather than on observational grounds.

The ionized medium near the GC also contains an even higher-temperature component (sometimes called the very hot ionized medium or VHIM), revealed by its hard X-ray thermal emission, both in a free-free continuum and in characteristic lines from highly ionized elements. Koyama et al. (1989) reported the detection with the Ginga satellite of intense 6.7-keV $\text{K}\alpha$ line emission from helium-like iron, the most abundant ionization state at a temperature of several keV. From the shape of the (supposedly free-free) continuum in the (2–18) keV energy band, they independently estimated the plasma temperature at $kT \sim 10 \text{ keV}$ (i.e., $T \sim 10^8 \text{ K}$). Yamauchi et al. (1990) then performed a two-dimensional mapping of the very hot 6.7-keV emitting plasma (outside the Galactic ridge). They found that its two-dimensional distribution on the plane of the sky could be fitted by an elliptical Gaussian with FWHM size $\simeq 270 \text{ pc} \times 150 \text{ pc}$ and major axis tilted clockwise by $\simeq 21^\circ$ with respect to the Galactic plane.

Subsequent, higher-energy-resolution observations in the (2–10) keV band with the ASCA satellite confirmed the presence of very hot plasma in the GC region (Koyama et al. 1996). Although the X-ray continuum could again be explained by thermal free-free emission at $kT \gtrsim 10 \text{ keV}$, the simultaneous appearance in the spectra of $\text{K}\alpha$ lines from helium-like and hydrogen-like ions of various elements suggests that the very hot plasma is either multi-temperature or out of ionization equilibrium. Its electron density was

estimated by Koyama et al. (1996) at $\sim (0.3 - 0.4) \text{ cm}^{-3}$. When integrated over an ellipsoid Gaussian distribution with FWHM size $\simeq (270 \text{ pc})^2 \times 150 \text{ pc}$ (from Yamauchi et al. 1990), this electron density implies a total H^+ mass $\sim (8 - 11) \times 10^4 M_\odot$, 58% of which lies inside $r = 150 \text{ pc}$. From this, we may conclude that the very hot gas encloses $\sim 7\% - 10\%$ of the ionized gas, and hence $\sim 0.3\% - 0.5\%$ of all the interstellar gas, inside $r = 150 \text{ pc}$.

3. Dynamical models

The observed non-axisymmetric distribution and non-circular motions of interstellar gas near the GC can most likely be attributed to the presence of a Galactic bar, and to a large extent, they can be explained in terms of the theoretical properties of stable closed orbits in the gravitational potential of a barred galaxy (see Binney & Merrifield 1998 for a brief review). Both analytical and numerical calculations of particle orbits in a barred gravitational potential have brought to light the existence of two families of stable closed orbits. Although the exact status of these two families depends on the shape and strength of the bar and can become rather complex, for our purposes it suffices to be aware of the basic typical situation. Typically, the orbits prevailing inside the bar's inner Lindblad resonance (ILR) are the so-called x_2 orbits, elongated perpendicular to the bar's major axis, and the orbits prevailing outside the ILR are the x_1 orbits, generally elongated along the bar – except between the bar's corotation radius and its outer Lindblad resonance (OLR), where most closed orbits are unstable (see, e.g., Contopoulos & Mertzaniades 1977;⁸ Contopoulos & Papayannopoulos 1980; Athanassoula 1992a). The ellipticity of both families of orbits increases toward the ILR, and on the whole x_1 orbits are more elongated than x_2 orbits.

Binney et al. (1991) proposed a dynamical model of interstellar gas in the innermost (2–3) kpc of the Galaxy meant to reproduce at best the observed morphology and kinematics of CO, CS and HI emissions. The basic scenario underlying their model is the following: Interstellar gas subject to the gravitational potential of the bar tends to settle onto stable closed orbits, although due to diverse dissipation processes, it gradually drifts inward through a sequence of decreasing-energy orbits. Gas starting off outside the ILR travels along x_1 orbits until its inward drift brings it to a cusped x_1 orbit, interior to which x_1 orbits become self-intersecting at their apocenters. Shocks and material collisions along the cusped and outermost self-intersecting x_1 orbits cause the gas to abruptly lose energy and angular momentum and to drop onto the lower-energy x_2 orbits, along which it continues its spiraling motion toward the GC. Since x_2 orbits are overall rounder than x_1 orbits, gas loses energy and drifts inward less rapidly in the “ x_2 disk”, which therefore attains higher densities.

Binney et al. (1991) interpreted the observational longitude-velocity (l, v) diagrams of CO and HI emissions in terms of the theoretical (l, v) curves generated by non self-intersecting x_1 orbits and by x_2 orbits. The cornerstone of their discussion is the parallelogram that encloses most of the emission in the CO (l, v) diagram (this parallelogram

⁸ It is interesting to note that the x_1 versus x_2 terminology in use today is opposite to that initially introduced by Contopoulos & Mertzaniades (1977) in the case of a weak bar.

corresponds to the 180-pc molecular ring discussed earlier, which, as we already mentioned, is also known as the “expanding molecular ring”). Binney et al. argued that the parallelogram could be identified with the (l, v) trace of the cusped x_1 orbit, thereby placing the GC molecular disk (i.e., the GC disk population of dense molecular clouds) on x_2 orbits. No such parallelogram appears in the H I (l, v) diagram, whose structure suggests instead that atomic gas extends well into the region of non self-intersecting x_1 orbits. These considerations led Binney et al. to propose that a substantial fraction of the interstellar gas turns molecular at the strong shocks present in the vicinity of the cusped x_1 orbit. Farther out, the observed gap in the interstellar gas distribution between radii ~ 1.5 kpc and ~ 3 kpc could presumably be explained by the generally unstable character of particle orbits in a region extending radially from somewhere inside corotation to the OLR and by the resulting expulsion of gas away from the unstable region. The accumulation of expelled gas just outside the OLR would then lie at the root of the Galactic disk molecular ring.

Detailed quantitative comparisons between the observational (l, v) diagrams and the theoretical (l, v) curves enabled Binney et al. (1991) to place constraints on the parameters of their model. The best constrained parameter is the inclination angle of the bar’s major axis to the line of sight, which was found to be $\theta_{\text{bar}} \simeq 16^\circ$ (within a few degrees) toward positive longitudes. Much more uncertain are the bar’s dimensions; Binney et al. arbitrarily adopted $a_0 = 1.2$ kpc for the bar’s semi-major axis (more exactly, the radius along the major axis beyond which the matter’s density falls off very steeply) and $4 : 3 : 3$ for the axis ratios, but the bar could easily be longer and more elongated. The bar’s corotation radius was arbitrarily set to $r_{\text{CR}} = 2.4$ kpc, consistent with the notions that the bar terminates somewhat inside corotation (Contopoulos & Papayannopoulos 1980; Sellwood & Sparke 1988; Athanassoula 1992b) and that the region around corotation is depopulated of gas.

For all its successes, Binney et al.’s (1991) model leaves a number of important observational features unexplained. Most notably, the longitudinal lopsidedness in the observed CO distribution is much more pronounced than the asymmetry expected from the bar’s inclination toward positive longitudes. In addition, Binney et al. noted a significant discrepancy in the velocity scales of the observational CO and H I (l, v) diagrams, when interpreted in the framework of their model. They attributed this discrepancy to the neglect of gas-dynamical effects in their particle-orbit approach, arguing that hydrodynamical forces at the strong shocks responsible for the transition from x_1 to x_2 orbits near the ILR lead to large departures from ballistic trajectories.

This argument prompted Jenkins & Binney (1994) to simulate interstellar gas flows in Binney et al.’s (1991) bar model. They tested two radically different two-dimensional, sticky-particle schemes, which neglect self-gravity, but allow for both accretion of matter shed by bulge stars and removal of clouds from regions above a given density threshold. Both schemes yield similar results, which qualitatively confirm the dynamical scenario envisioned by Binney et al., with one important difference. Here it is found that gas parcels approaching (but still outside) the cusped x_1 orbit tumble onto x_2 orbits located deeper inside, so that a nearly empty zone develops near the cusped orbit between the “ x_1 ring” and the “ x_2 disk”. Only an external source of matter, such as gas loss by bulge stars, can keep this tran-

sition zone appreciably populated. For future reference, the ILR lies at $r_{\text{ILR}} \simeq 350$ pc, the cusped orbit has a half-size $\simeq 650$ pc \times 150 pc, and for reasonable values of the numerical parameters, the inner boundary of the x_1 ring has a half-size $\simeq (750 \pm 50)$ pc \times (400 ± 50) pc and the x_2 disk a half-size $\simeq (280 \pm 20)$ pc \times (180 ± 20) pc.

Regrettably, Jenkins & Binney’s (1994) simulations fail to resolve the main problems with Binney et al.’s (1991) model, namely, its inability to reproduce the pronounced lopsidedness in the observed CO distribution and its inability to simultaneously explain the observational CO and H I (l, v) diagrams. Jenkins & Binney suggested that part of the blame could probably be laid on the limitations of their numerical schemes, which are restricted to two dimensions and omit self-gravity. They also pointed out that the unsteadiness of gas flows near the ILR could be partly (though certainly not entirely) responsible for the observed asymmetry in CO. Finally, they raised the possibility that CO and H I line emissions might not be reliable tracers of interstellar gas mass.

Subsequently, many hydrodynamical simulations of gas flows in barred gravitational potentials were performed with various numerical techniques. Englmaier & Gerhard (1999) employed a two-dimensional smoothed-particle hydrodynamics code to follow interstellar gas flows in the Galactic gravitational potential deduced from the deprojected and dust-corrected COBE/DIRBE near-infrared luminosity distribution (see Binney et al. 1997), under the assumption of a constant mass-to-light ratio. The COBE data imply that the bar’s inclination angle is restricted to the interval $15^\circ - 35^\circ$, with a preferred value $\theta_{\text{bar}} = 20^\circ$. With this value, the bar has a semi-major axis $a \sim 2$ kpc and axis ratios $\simeq 5 : 3 : 2$, it is surrounded by a thin elliptical disk with radius ~ 3.5 kpc along the major axis and ~ 2 kpc along the minor axis, and corotation occurs at $r_{\text{CR}} \simeq 3$ kpc (assuming $r_\odot = 8$ kpc; Binney et al. 1997). Englmaier & Gerhard (1999) supplemented the gravitational potential deduced from the COBE near-infrared luminosity with the contributions from a central cusp and (for some runs) an outer dark halo. They presented their simulation results in the form of face-on surface-density maps of interstellar gas in the inner Galaxy ($r < r_\odot$) together with the associated (l, v) diagrams. The maps clearly feature a four-armed spiral pattern outside corotation and two pairs of arms inside corotation, each pair emanating approximately from one end of the bar. Interior to the two innermost arms, the vicinity of the cusped x_1 orbit becomes rapidly depleted, as gas parcels reaching the cusped orbit’s shock quickly fall in along the shock ridges onto the central x_2 disk. The latter stands out in the surface-density maps as a compact disk of radius ~ 150 pc.

Bissantz et al. (2003) ran similar hydrodynamical simulations based on the improved near-infrared luminosity distribution models of Bissantz & Gerhard (2002). In the best-fit model that they adopted, the bar’s inclination angle is again $\theta_{\text{bar}} = 20^\circ$, but its semi-major axis is now $a \simeq 1.75$ kpc, its axis ratios $\simeq 5 : 2 : 1.5$ and its corotation radius $r_{\text{CR}} \simeq 3.4$ kpc (assuming again $r_\odot = 8$ kpc). Bissantz et al. (2003) examined the gas dynamics in the bar region more closely. As a starting point, they computed closed x_1 and x_2 orbits in their model gravitational potential and found that the outermost x_2 orbit does not reach out to the cusped x_1 orbit. This, they argued, could be the reason why a gap opens up in the simulations between the

cusped orbit and the x_2 disk. According to their calculations, the cusped orbit has a half-size $\simeq 1.35 \text{ kpc} \times 280 \text{ pc}$ (approximately twice as large as in Jenkins & Binney 1994) and the outermost closed x_2 orbit has a half-size $\simeq 175 \text{ pc} \times 85 \text{ pc}$ (nearly twice smaller than the half-size of the x_2 disk in Jenkins & Binney 1994).

All the above simulations have two important limitations: they are two-dimensional and, more critically, the Galactic gravitational potential is prescribed at the outset and taken to be time-independent and point-symmetric with respect to the GC. A major improvement on both counts was brought by Fux (1999), who performed three-dimensional, self-consistent composite simulations of the inner Galaxy, in which the stellar bar and the interstellar gas are evolved in concert, with N -body and smoothed-particle hydrodynamics codes, respectively. All gravitational interactions (including self-gravity) are taken into account, and no stationarity or symmetry condition is imposed. The simulated face-on surface-density maps are found to fluctuate in time. The stellar bar varies in shape and its center of mass oscillates around the GC with an amplitude of several 100 pc. The interstellar gas flow is unsteady and asymmetric; it develops transient spiral arms and shock fronts as well as a ring or disk of x_2 orbits which closely follows the bar's center of mass.

Fux (1999) constrained the location of the Sun relative to the bar with the help of dust-corrected COBE/DIRBE K-band data. Moreover, he constructed movies of synthetic (l, v) diagrams, compared them to the observational CO and H I (l, v) diagrams and selected the best-matching snapshots. He then used the corresponding gas flow models to interpret the main features of the observational (l, v) diagrams. The two preferred models have $\theta_{\text{bar}} \simeq 25^\circ$ (compatible with the COBE data) and $r_{\text{CR}} \simeq 4.5 \text{ kpc}$. In the model that Fux singled out for attention (the one that gives the best overall agreement with the (l, v) observations), the cusped x_1 orbit has a half-size $\simeq 3.2 \text{ kpc} \times 1.3 \text{ kpc}$, which is considerably larger than in the simulations described above. With such large dimensions, the cusped orbit cannot possibly correspond to the parallelogram in the observational CO (l, v) diagram, as suggested by Binney et al. (1991). Instead, Fux's conjecture is that the parallelogram could represent interstellar gas streams originating from the cusped orbit or from dustlanes (associated with "off-axis shocks") connecting the cusped orbit to the x_2 ring/disk, and grazing the x_2 ring/disk. Aside from this new interpretation, Fux pointed out that the bar parameters cannot be estimated with any confidence from the best-matching models, and he devised a model-independent method relying on purely geometric considerations. This method yields $\theta_{\text{bar}} = 25^\circ \pm 4^\circ$ for the bar's inclination angle, $a \simeq 3.2 \text{ kpc}$ for its semi-major axis, $a : b \simeq 5 : 3$ for its face-on axis ratio and $r_{\text{CR}} \simeq (4.0 \pm 0.5) \text{ kpc}$ for its corotation radius (assuming $r_\odot = 8 \text{ kpc}$).

A great merit of Fux's (1999) study is that it underscores the inherent non-stationarity of the Galactic bar, with its large-amplitude oscillations around the GC, and the resulting unsteadiness and off-centering of the interstellar gas distribution. In this manner, it offers a natural explanation for the observed longitudinal asymmetry in the CO intensity maps. Furthermore, since the cusped x_1 orbit is no longer associated with the parallelogram in the CO (l, v) diagram, the difference in the velocity scales of the observational CO and H I (l, v) diagrams no longer poses a

problem. On the other hand, Fux's simulations raise their own set of questions, as the large values obtained for the corotation radius and for the dimensions of the cusped orbit seem difficult to reconcile with the observed gas deficit between $r \sim 1.5 \text{ kpc}$ and 3 kpc and with the Galactic disk molecular ring starting at $r \simeq 3.5 \text{ kpc}$.

Another, more subtle aspect of the interstellar gas morphology near the GC concerns the orientation of the central x_2 ring/disk with respect to the bar's major axis. We know that closed particle (i.e., collisionless) orbits in a barred gravitational potential are elongated either parallel or perpendicular to the bar's major axis. Typically, they are elongated parallel to the bar between the ILR and corotation and outside the OLR, and perpendicular to the bar inside the ILR (where the central x_2 ring/disk resides) and between corotation and the OLR (e.g., Contopoulos & Mertzaniides 1977; Contopoulos & Papayannopoulos 1980). This is not true of closed gas (i.e., collisional) orbits. Once pressure and viscous forces are taken into account, the 90° jumps in orbit orientation at the bar's resonances are completely smoothed out. Wada (1994), who studied the case of a weak bar with an analytical damped-oscillator model, found that the orbit inclination angle to the bar's major axis, $\Delta\theta$, varies gradually with radius, such that $0^\circ < \Delta\theta \leq 45^\circ$ between the ILR and corotation and outside the OLR, and $45^\circ \leq \Delta\theta < 90^\circ$ inside the ILR and between corotation and the OLR. Hence, x_2 orbits lead the bar by $\Delta\theta > 45^\circ$, and the whole x_2 ring/disk should appear inclined to the bar by a little more than 45° . This is exactly what a close scrutiny of the face-on maps of Englmaier & Gerhard (1999) and Fux (1999) shows. In addition, if the bar is itself inclined by $\theta_{\text{bar}} \simeq 20^\circ - 25^\circ$ to the line of sight (Englmaier & Gerhard 1999; Fux 1999; Bissantz et al. 2003), the x_2 ring/disk should be inclined by $\simeq 70^\circ$ to the line of sight, in excellent agreement with the observational conclusions of Sawada et al. (2004). Let us also note that the gradual variation in orbit inclination with radius automatically gives rise to spiral density enhancements. One could surmise that these enhancements are related to the molecular arms discussed by Sofue (1995a) (see section 2.2).

4. Our model for the gas distribution

It is clear that our observational knowledge of the interstellar gas distribution in the GB is rather patchy. Although theoretical models can probably bridge some of the gaps, there remain important murky areas. In this section, we gather the relevant observational results (see section 2) that we deem the most trustworthy, we complement them with some theoretical predictions from gas dynamical models (see section 3) and we try to piece everything together into a coherent picture of the interstellar gas distribution in the innermost 3 kpc of our Galaxy.

4.1. The central molecular zone

There have been several attempts to deproject sky maps of molecular line emission in the CMZ. In most cases, a gas kinematic model is appealed to in order to transform the measured line-of-sight velocity into line-of-sight distance. Unfortunately, our poor knowledge of the true gas kinematics near the GC renders this kind of method unreliable.

A notable exception is the work of Sawada et al. (2004), who derived a face-on map of the molecular gas without

any kinematic assumption, on the sole basis of observational (emission *versus* absorption) data (see section 2.2). For this reason, their face-on map will serve as the first building block of our model. Thus, we assume that the CMZ projected onto the Galactic plane has the shape of a 500 pc \times 200 pc ellipse inclined by 70° to the line of sight toward positive longitudes. From Sawada et al.’s Figure 10a, we estimate that the ellipse is centered on $(x_c, y_c) \simeq (-50 \text{ pc}, 50 \text{ pc})$.⁹ The peak in surface density appears displaced eastward from the ellipse center, to $\sim (-30 \text{ pc}, 100 \text{ pc})$, but in view of the large uncertainties involved in the deprojection, the apparent peak position should not be taken at face value. It is even possible that the molecular gas is in fact distributed in a ring rather than a disk (e.g., Sofue 1995a). While we do not rule out this possibility, we find the present observational evidence inconclusive. Theoretical studies are not of great help either. Accepting the idea that the CMZ corresponds to the domain of x_2 orbits (see section 3), we note that both x_2 disks and x_2 rings have come up in hydrodynamical simulations (e.g., Jenkins & Binney 1994; Englmaier & Gerhard 1999; Fux 1999).

Here, as a simple compromise, we adopt a nearly flat (i.e., between peaked and ring-like) horizontal distribution of the type utilized by Launhardt et al. (2002) for their warm inner disk (Equation 1). For convenience, we introduce horizontal coordinates in the CMZ frame, (X, Y) , defined such that X is along the major axis and Y along the minor axis. The CMZ coordinates (X, Y) are then related to the Galactic coordinates (x, y) through

$$\begin{cases} X = (x - x_c) \cos \theta_c + (y - y_c) \sin \theta_c \\ Y = -(x - x_c) \sin \theta_c + (y - y_c) \cos \theta_c \end{cases} \quad (15)$$

with $x_c = -50 \text{ pc}$, $y_c = 50 \text{ pc}$ and $\theta_c = 70^\circ$ (see Figure 2). Adjusting the horizontal profile from Equation 1 to an elliptical disk with semi-major axis 250 pc and axis ratio 2.5 gives for the H_2 space-averaged density in the CMZ

$$\langle n_{\text{H}_2} \rangle_{\text{CMZ}} \propto \exp \left[- \left(\frac{\sqrt{X^2 + (2.5 Y)^2} - X_c}{L_c} \right)^4 \right], \quad (16)$$

where $X_{\text{max}} = 250 \text{ pc}$, $X_c = X_{\text{max}}/2 = 125 \text{ pc}$ and $L_c = X_{\text{max}}/(2 (\ln 2)^{1/4}) \simeq 137 \text{ pc}$. Evidently, Equation 16 can easily be adapted to a larger/smaller CMZ or to a more/less elongated CMZ by increasing/decreasing the value of X_{max} or the prefactor of Y , respectively. It can also be adapted to a ring morphology by increasing X_c/X_{max} and decreasing L_c/X_{max} accordingly.

Sawada et al. (2004) provided only a face-on view of the molecular gas, with no information on its vertical distribution or density scale. Regarding the vertical distribution, one has to distinguish between the GC molecular disk and the surrounding 180-pc molecular ring (see section 2.2). The GC molecular disk appears planar and closely aligned with the Galactic plane (Heiligman 1987; Bally et al. 1988; Burton & Liszt 1992; Oka et al. 1998). Its FWHM thickness is typically $\sim 15 - 30 \text{ pc}$, with a tendency to increase outward (up to $\sim 50 \text{ pc}$) as well as toward massive molecular complexes (up to $\sim 30 - 60 \text{ pc}$) (Heiligman 1987; Bally

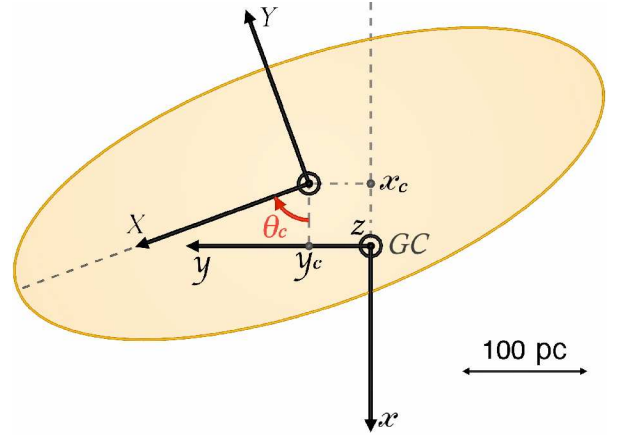


Fig. 2. Face-on view of our CMZ. (x, y, z) are the Galactocentric coordinates and (X, Y) the CMZ horizontal coordinates. The CMZ is elliptical, 500 pc \times 200 pc in size, centered on $(x_c, y_c) = (-50 \text{ pc}, 50 \text{ pc})$ and inclined by $\theta_c = 70^\circ$ to the line of sight.

et al. 1988; Sofue 1995a; Burton & Liszt 1992). Here, following Burton & Liszt (1992), we ignore the spatial variations of the disk thickness, which we set to 30 pc, and we assume a Gaussian vertical distribution:

$$\langle n_{\text{H}_2} \rangle_{\text{CMZ}} \propto \exp \left[- \left(\frac{z}{H_c} \right)^2 \right], \quad (17)$$

with $H_c = (30 \text{ pc})/(2 \sqrt{\ln 2}) \simeq 18 \text{ pc}$. The 180-pc molecular ring is thicker than the GC molecular disk (Bally et al. 1988; Sofue 1995b), consistent with the outward increase in the GC molecular disk’s thickness noted above, with the flaring of the H_2 disk of Burton & Liszt (1992) and with the greater scale height obtained by Sanders et al. (1984) for the H_2 GB disk as a whole ($r \lesssim 1.3 \text{ kpc}$). In addition, the 180-pc molecular ring is tilted out of the Galactic plane, counterclockwise by $\sim 5^\circ - 9^\circ$ (Heiligman 1987). It is also inclined to the line of sight, as implied by the fact that its negative-velocity portion (near side) lies at negative latitudes, while its positive-velocity portion (far side) lies at positive latitudes (Heiligman 1987; Bally et al. 1988). Heiligman (1987) estimated an inclination angle $\sim 85^\circ$ to the plane of the sky, whereas from Figure 11 of Bally et al. (1988) together with the attendant discussion we estimate an inclination angle $\sim 80^\circ$. It is noteworthy that both the tilt and the inclination of the 180-pc molecular ring are in the same sense as those of the GB disk (see section 2.2 for the molecular GB disk and section 2.3 for the H I GB disk). In any event, since the 180-pc molecular ring actually contains but a small fraction of the CMZ mass, we will not treat it separately from the GC molecular disk.

We now turn to the H_2 density scale, which can be inferred from the total H_2 mass of the CMZ. Our H_2 mass estimates (assuming $X_{\text{CO}} = 5 \times 10^{19} \text{ cm}^{-2} \text{ K}^{-1} \text{ km}^{-1} \text{ s}$) for various regions of the GB are summarized in Table 4. Clearly, none of the listed region corresponds exactly to our CMZ, whose projected half-size is $250 \text{ pc} \times \sin 70^\circ \simeq 235 \text{ pc}$. The closest is the region $r \lesssim 200 \text{ pc}$ studied by Sofue (1995ab), which contains $\sim 1.3 \times 10^7 M_\odot$ of H_2 in the GC molecular disk plus $\sim 2.7 \times 10^6 M_\odot$ of H_2 in the 180-pc molecular ring, i.e., a total H_2 mass $\sim 1.6 \times 10^7 M_\odot$. From this, we estimate that our CMZ has an H_2 mass

⁹ The (x, y, z) coordinate system used by Sawada et al. (2004) is equivalent to our (x, y, z) system (see Figure 1) rotated clockwise by 90° .

$\sim 1.9 \times 10^7 M_\odot$. This value is in good agreement with the H_2 mass of the GB region $r_\perp \lesssim 375$ pc being $\sim (4.2 - 4.4) \times 10^7 M_\odot$ (Oka et al. 1998; Sodroski et al. 1995; see Table 4) and with the total hydrogen mass of the region $r \lesssim 230$ pc being $\sim 2 \times 10^7 M_\odot$ (Launhardt et al. 2002; see Table 1).

The H_2 density scale can now be obtained by integrating the density model described by Equations 16 and 17 over the relevant region and equating the integral to our estimated H_2 mass of $1.9 \times 10^7 M_\odot$. The result is $(\langle n_{H_2} \rangle_{\text{CMZ}})_{\text{max}} \simeq 150 \text{ cm}^{-3}$, so that the H_2 space-averaged density in the CMZ can be written as

$$\langle n_{H_2} \rangle_{\text{CMZ}} = (150 \text{ cm}^{-3}) \exp \left[- \left(\frac{\sqrt{X^2 + (2.5Y)^2} - X_c}{L_c} \right)^4 \right] \times \exp \left[- \left(\frac{z}{H'_c} \right)^2 \right], \quad (18)$$

where $X_c = 125$ pc, $L_c = 137$ pc, $H_c = 18$ pc and (X, Y) are the CMZ horizontal coordinates defined by Equation 15. On the plane of the sky, the CMZ appears as a $474 \text{ pc} \times 30 \text{ pc}$ (size at half-maximum density) ellipse, displaced eastward by 50 pc, so that it extends out to $r_\perp = 287$ pc at positive longitudes and $r_\perp = 187$ pc at negative longitudes (see Figure 4a).

For the atomic gas, all the face-on maps deduced from 21-cm observations rely on a number of kinematic assumptions, which render them questionable. Therefore, we prefer to take an alternative approach, based on our more solid knowledge of the molecular gas distribution and on the premise that atomic and molecular gases are similarly distributed in space (as argued by Liszt & Burton 1996). The only obvious difference between both gases concerns the thickness of their layer, which is ~ 30 pc for H_2 (see above Equation 17) and ~ 90 pc for HI (Rohlfs & Braunsfurth 1982; see section 2.3). Thus, we adopt for HI the same horizontal and vertical profiles as for H_2 (Equations 16 and 17, respectively), with this difference that $H_c \rightarrow H'_c = (90 \text{ pc}) / (2\sqrt{\ln 2}) \simeq 54$ pc.

The HI mass of the CMZ is very uncertain. As we mentioned in section 2.3, current HI mass estimates differ by up to a factor ~ 5 . Here, we favor the mass estimates of Rohlfs & Braunsfurth (1982), who directly focused on a region comparable in size to our CMZ – as opposed to Burton & Liszt (1978, 1993) and Liszt & Burton (1980), who studied the GB disk as a whole. Rohlfs & Braunsfurth (1982) derived an HI mass $\sim 3.1 \times 10^6 M_\odot$ for the region $r \lesssim 300$ pc, which translates into an HI mass $\sim 1.4 \times 10^6 M_\odot$ for the region $r \lesssim 200$ pc. Since the H_2 mass in the latter region is $\sim 1.6 \times 10^7 M_\odot$ (Sofue 1995ab; see paragraph preceding Equation 18), we may conclude that the HI mass amounts to 8.8% of the H_2 mass.

With three times the scale height and 8.8% of the mass of the molecular gas, the atomic gas reaches only 2.9% of its maximum mass density, or 5.8% of its maximum number density, i.e., $(\langle n_{\text{HI}} \rangle_{\text{CMZ}})_{\text{max}} \simeq 8.8 \text{ cm}^{-3}$. Altogether, the HI

space-averaged density in the CMZ is given by

$$\langle n_{\text{HI}} \rangle_{\text{CMZ}} = (8.8 \text{ cm}^{-3}) \exp \left[- \left(\frac{\sqrt{X^2 + (2.5Y)^2} - X_c}{L_c} \right)^4 \right] \times \exp \left[- \left(\frac{z}{H'_c} \right)^2 \right], \quad (19)$$

with $H'_c = 54$ pc and X_c , L_c , (X, Y) as defined below Equation 18 (see Figure 4b).

4.2. The “holed” GB disk

We saw in section 4.1 that reliable observational information on the interstellar gas distribution inside the CMZ is scanty. It turns out that the observational situation is even worse outside the CMZ. It is true that a number of tilted GB disk models have been constructed on the basis of CO and 21-cm observations (see sections 2.2 and 2.3), but all of them involve unverified assumptions, both on the overall geometry (e.g., axial symmetry) and on the gas kinematics.

The model that we consider the most plausible, despite its inherent uncertainties, is that of Liszt & Burton (1980), because it is the only model with an elongated disk, which makes it the easiest to reconcile with our theoretical understanding of gas dynamics in the GB (see section 3). Indeed, the GB disk outside the CMZ is believed to correspond to the domain of non self-intersecting x_1 orbits, which form an elongated, radially thick ring around the x_2 disk/ring (itself identified with the CMZ). In some hydrodynamical simulations, the inner boundary of the x_1 ring grazes the x_2 disk/ring, while in others, a gap opens up between both.

Here, we start from Liszt & Burton’s (1980) GB disk, namely, an elliptical disk with semi-major axis 1.6 kpc and axis ratio 3.1, and we introduce a hole in the middle just large enough to enclose the CMZ. It can be checked that a hole with the same shape and half the size of the entire GB disk is sufficient for our purpose. Then the inner boundary of the “holed” GB disk has a half-size of $800 \text{ pc} \times 258 \text{ pc}$, in reasonably good agreement with the results of hydrodynamical simulations. For instance, Jenkins & Binney (1994) found that the inner boundary of the x_1 ring has a half-size $\simeq (750 \pm 50) \text{ pc} \times (400 \pm 50) \text{ pc}$. The x_1 ring is more difficult to make out in the larger-scale simulated maps of Englmaier & Gerhard (1999) and of Bissantz et al. (2003), but its inner boundary clearly appears more elongated, with an axis ratio possibly close to our adopted value of 3.1. Let us also point out that our GB disk is more elongated than our CMZ (whose axis ratio is 2.5; see section 4.1). This is perfectly consistent not only with gas flow simulations, but also with particle orbit calculations, which predict a greater ellipticity for x_1 orbits than for x_2 orbits (see first paragraph of section 3).

According to Liszt & Burton (1980), the GB disk is tilted by $\alpha = 13^\circ.5$ out of the Galactic plane [counterclockwise rotation by α about the x -axis, whereby $(x, y, z) \rightarrow (x, y', z')$] and inclined by $i = 70^\circ$ to the plane of the sky [“front-downward” rotation by $\beta = 90^\circ - i$ about the y' -axis, whereby $(x, y', z') \rightarrow (x'', y', z'')$], and the GB disk’s major axis forms an angle $\theta_d = 48^\circ.5$ to the x'' -axis [measured clockwise about the z'' -axis]. If we denote the spatial coordinates in the GB disk frame by $(\mathcal{X}, \mathcal{Y}, \mathcal{Z})$, with \mathcal{X} along the major axis, \mathcal{Y} along the minor axis and \mathcal{Z} along

the northern normal, the transformation from Galactic coordinates to GB disk coordinates reads

$$\begin{cases} \mathcal{X} = x \cos \beta \cos \theta_d \\ \quad - y (\sin \alpha \sin \beta \cos \theta_d - \cos \alpha \sin \theta_d) \\ \quad - z (\cos \alpha \sin \beta \cos \theta_d + \sin \alpha \sin \theta_d) \\ \mathcal{Y} = -x \cos \beta \sin \theta_d \\ \quad + y (\sin \alpha \sin \beta \sin \theta_d + \cos \alpha \cos \theta_d) \\ \quad + z (\cos \alpha \sin \beta \sin \theta_d - \sin \alpha \cos \theta_d) \\ \mathcal{Z} = x \sin \beta \\ \quad + y \sin \alpha \cos \beta \\ \quad + z \cos \alpha \cos \beta, \end{cases} \quad (20)$$

with $\alpha = 13^\circ.5$, $\beta = 20^\circ$ and $\theta_d = 48^\circ.5$ (see Figure 3).

Now that we have specified the horizontal shape and dimensions as well as the orientation of our holed GB disk, we may fit to it horizontal and vertical profiles of the same type as for our CMZ (Equations 16 and 17, respectively). Again, we assume that molecular and atomic gases are similarly distributed in space, except for a possible difference in scale height. Under these conditions, we can write

$$\begin{aligned} \langle n_{\text{H}_2} \rangle_{\text{disk}} &\propto \exp \left[- \left(\frac{\sqrt{\mathcal{X}^2 + (3.1 \mathcal{Y})^2} - \mathcal{X}_d}{L_d} \right)^4 \right], \\ \langle n_{\text{H I}} \rangle_{\text{disk}} &\propto \exp \left[- \left(\frac{\sqrt{\mathcal{X}^2 + (3.1 \mathcal{Y})^2} - \mathcal{X}_d}{L_d} \right)^4 \right], \end{aligned} \quad (21)$$

with $\mathcal{X}_{\text{max}} = 1.6$ kpc, $\mathcal{X}_{\text{min}} = 0.8$ kpc, $\mathcal{X}_d = (\mathcal{X}_{\text{max}} + \mathcal{X}_{\text{min}})/2 = 1.2$ kpc and $L_d = (\mathcal{X}_{\text{max}} - \mathcal{X}_{\text{min}})/(2 (\ln 2)^{1/4}) \simeq 438$ pc, and

$$\begin{aligned} \langle n_{\text{H}_2} \rangle_{\text{disk}} &\propto \exp \left[- \left(\frac{\mathcal{Z}}{H_d} \right)^2 \right], \\ \langle n_{\text{H I}} \rangle_{\text{disk}} &\propto \exp \left[- \left(\frac{\mathcal{Z}}{H'_d} \right)^2 \right]. \end{aligned} \quad (22)$$

For the scale height, we adopt $H_d = (70 \text{ pc})/(2\sqrt{\ln 2}) \simeq 42$ pc for H_2 (Sanders et al. 1984) and $H'_d = \sqrt{2}$ (85 pc) $\simeq 120$ pc for H I (Liszt & Burton 1980). Like in the CMZ, the atomic layer is about three times thicker than the molecular layer. Moreover, each layer is $\simeq 2.2 - 2.3$ times thicker in the holed GB disk than in the CMZ.

Our density model can again be normalized with the help of the total H_2 and H I masses in the considered region. The entire GB disk contains $\sim 5.3 \times 10^7 M_\odot$ of H_2 (Sanders et al. 1984; see Table 4) and $\sim 5.2 \times 10^6 M_\odot$ of H I (Liszt & Burton 1980; see Table 5), while our CMZ contains $\sim 1.9 \times 10^7 M_\odot$ of H_2 and $\sim 1.7 \times 10^6 M_\odot$ of H I (see section 4.1). By subtraction, we find that our holed GB disk has an H_2 mass $\sim 3.4 \times 10^7 M_\odot$ and an H I mass $\sim 3.5 \times 10^6 M_\odot$. We are fully aware of the pitfalls of this mass estimation, especially as the masses involved in the subtraction procedure have considerable uncertainty. Particularly uncertain is the H_2 mass of the entire GB disk. The only estimate available to us is the value from Sanders et al. (1984). But this value applies to an axisymmetric disk of radius 1.3 kpc having twice the surface area of our elliptical GB disk, which means that it could overestimate the true mass by up to a factor ~ 2 . On the other hand, the comparatively large values obtained by Sodroski et al.

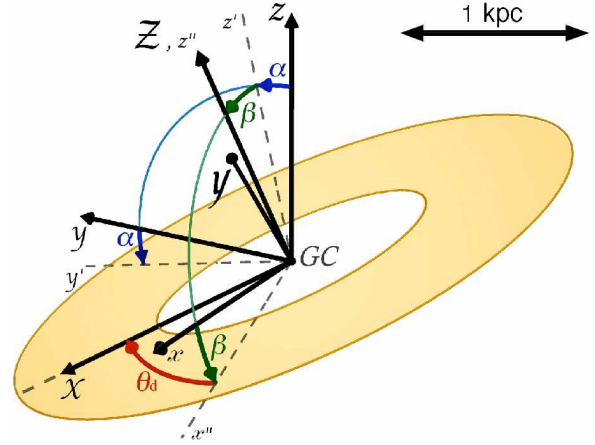


Fig. 3. Three-dimensional view of our holed GB disk. (x, y, z) are the Galactocentric coordinates, $(\mathcal{X}, \mathcal{Y}, \mathcal{Z})$ the GB disk coordinates, and (x, y', z') , (x'', y'', z'') the auxiliary coordinates defined above Equation 20. The holed GB disk is elliptical, 3.2 kpc long and $(3.2 \text{ kpc})/3.1 \simeq 1.03$ kpc wide, and its inner boundary has half the dimensions of its outer boundary. Relative to the Galactic plane, its principal plane is tilted by $\alpha = 13^\circ.5$ about the x -axis and inclined by $\beta = 20^\circ$ about the y' -axis, and its major axis is oriented at $\theta_d = 48^\circ.5$ to the x'' -axis.

(1995) and by Oka et al. (1998) for a smaller region (see Table 4) suggest instead that Sanders et al.'s (1984) value could underestimate the true mass by roughly the same factor. Hence, the two sources of error tend to counteract each other. In addition, two facts allow us to place some confidence in our results. First, the H_2 and H I masses of our holed GB disk are slightly smaller than what they would be if the gas were uniformly distributed throughout the GB disk ($\sim 4.0 \times 10^7 M_\odot$ and $\sim 3.9 \times 10^6 M_\odot$, respectively). Second, H I represents 8.8% by mass of H_2 in the CMZ and 10.3% in the holed GB disk. This statement supports Liszt & Burton's (1996) claim that both gases have similar spatial distributions, not only in the CMZ and in the holed GB disk separately (as we already assumed earlier), but also throughout the entire GB disk. It is also reassuring to obtain a slightly lower H I mass fraction in the CMZ.

If we now equate the space integral of Equation 21 times Equation 22 to our estimated H_2 and H I masses, we find $(\langle n_{\text{H}_2} \rangle_{\text{disk}})_{\text{max}} \simeq 4.8 \text{ cm}^{-3}$ and $(\langle n_{\text{H I}} \rangle_{\text{disk}})_{\text{max}} \simeq 0.34 \text{ cm}^{-3}$. Hence, the holed GB disk has an H_2 space-averaged density

$$\begin{aligned} \langle n_{\text{H}_2} \rangle_{\text{disk}} &= (4.8 \text{ cm}^{-3}) \exp \left[- \left(\frac{\sqrt{\mathcal{X}^2 + (3.1 \mathcal{Y})^2} - \mathcal{X}_d}{L_d} \right)^4 \right] \\ &\quad \times \exp \left[- \left(\frac{\mathcal{Z}}{H_d} \right)^2 \right] \end{aligned} \quad (23)$$

and an H I space-averaged density

$$\begin{aligned} \langle n_{\text{H I}} \rangle_{\text{disk}} &= (0.34 \text{ cm}^{-3}) \exp \left[- \left(\frac{\sqrt{\mathcal{X}^2 + (3.1 \mathcal{Y})^2} - \mathcal{X}_d}{L_d} \right)^4 \right] \\ &\quad \times \exp \left[- \left(\frac{\mathcal{Z}}{H'_d} \right)^2 \right], \end{aligned} \quad (24)$$

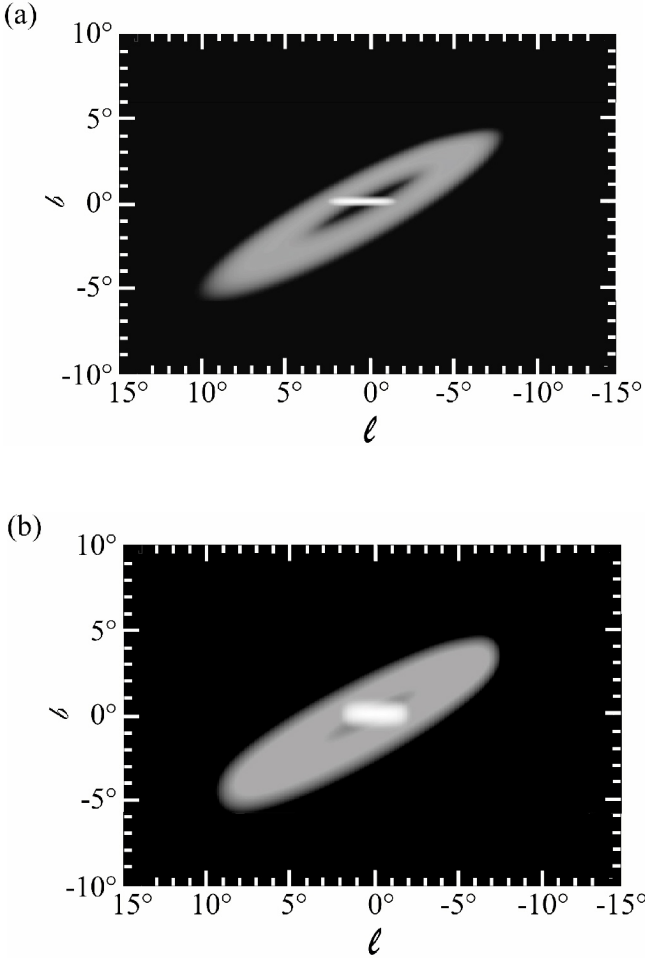


Fig. 4. Projection of the CMZ (bright area) and the holed GB disk (fainter area) onto the plane of the sky: (a) molecular gas (see Equations 18 and 23); (b) atomic gas (see Equations 19 and 24). The apparent sizes are a little larger than the sizes at half-maximum density, because of the logarithmic scale used in the projection. In contrast to the CMZ, which is truly displaced to the left, the GB disk is symmetric with respect to the GC, and the only reason why it appears more extended on the left side is because its positive-longitude portion lies closer to us.

with $\mathcal{X}_d = 1.2$ kpc, $L_d = 438$ pc, $H_d = 42$ pc and $H'_d = 120$ pc. On the plane of the sky, the GB disk extends out to $r_\perp = 1.14$ kpc (radius at half-maximum density) on each side of the GC (see Figure 4). Projected onto the Galactic plane, it has the shape of a 2.94 kpc \times 1.02 kpc (FWHM size) ellipse inclined clockwise by 47.6° to the line of sight (see Figure 5). This inclination angle is greater than that typically found for the Galactic stellar bar ($\theta_{\text{bar}} \simeq 15^\circ - 35^\circ$; see section 3), but it is in good agreement with the value $\theta_{\text{bar}} = 44^\circ \pm 10^\circ$ recently obtained by Benjamin et al. (2005) from the GLIMPSE Point Source Catalog.

4.3. The ionized component

The best available model for the spatial distribution of interstellar free electrons in the GB is the NE2001 model of Cordes & Lazio (2002) presented in section 2.4. According to this model, the total mass of interstellar ionized hydrogen in the region $r \leq 3$ kpc is $(7.3 \times 10^7 M_\odot) / (1 + 0.2 f_{\text{HIM}})$,

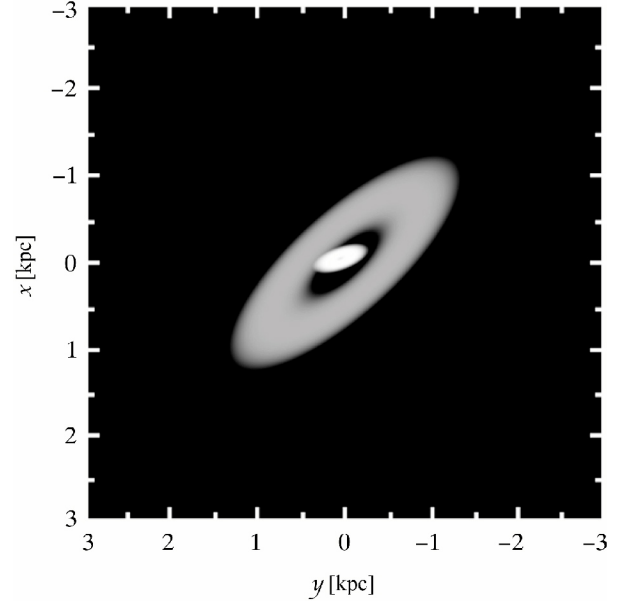


Fig. 5. Projection of the CMZ (bright area) and the holed GB disk (fainter area) onto the Galactic plane. Displayed here is the H_2 map (from Equations 18 and 23). The H I map (from Equations 19 and 24) looks identical, except for this hardly noticeable difference that the GB-disk-to-CMZ luminosity ratio is slightly greater. For the same reason as in Figure 4, the apparent sizes are a little larger than the sizes at half-maximum density.

where f_{HIM} is the fraction of ionized gas belonging to the hot medium (see Table 6). The mass of hot H^+ in the same region can be estimated from Almy et al.'s (2000) model (neglecting the contribution from very hot H^+) at $1.2 \times 10^7 M_\odot$ (see Table 6). It then follows that $f_{\text{HIM}} = 17\%$ (or, equivalently, $f_{\text{WIM}} = 83\%$) and that the total mass of H^+ inside 3 kpc is $7.1 \times 10^7 M_\odot$, divided between $5.9 \times 10^7 M_\odot$ in the WIM and $1.2 \times 10^7 M_\odot$ in the HIM. Furthermore, from Equation 11 with $f_{\text{HIM}} = 17\%$, we gather that the H^+ space-averaged density is given by $\langle n_{\text{H}^+} \rangle = 0.97 \langle n_e \rangle$. The partial contributions from the warm and hot ionized media are globally given by $\langle n_{\text{H}^+} \rangle_{\text{WIM}} = f_{\text{WIM}} \langle n_{\text{H}^+} \rangle$ and $\langle n_{\text{H}^+} \rangle_{\text{HIM}} = f_{\text{HIM}} \langle n_{\text{H}^+} \rangle$, respectively. For the WIM, which contributes a large 83% of the total H^+ mass, we may reasonably assume that the above global relation remains approximately valid locally. Owing to the large uncertainties in the exact spatial dependence of the density distributions, we feel that taking $\langle n_{\text{H}^+} \rangle_{\text{WIM}} = f_{\text{WIM}} \langle n_{\text{H}^+} \rangle$ at all \mathbf{r} is safer than subtracting $\langle n_{\text{H}^+} \rangle_{\text{HIM}}$ (which can be estimated independently; see next paragraph) from $\langle n_{\text{H}^+} \rangle$. In that case, the H^+ space-averaged density of the WIM is simply $\langle n_{\text{H}^+} \rangle_{\text{WIM}} = 0.80 \langle n_e \rangle$ or, in view of Equations 7 – 10,

$$\begin{aligned} \langle n_{\text{H}^+} \rangle_{\text{WIM}} = & (8.0 \text{ cm}^{-3}) \\ & \times \left\{ \exp \left[-\frac{x^2 + (y - y_3)^2}{L_3^2} \right] \exp \left[-\frac{(z - z_3)^2}{H_3^2} \right] \right. \\ & + 0.009 \exp \left[-\left(\frac{r - L_2}{L_2/2} \right)^2 \right] \text{sech}^2 \left(\frac{z}{H_2} \right) \\ & \left. + 0.005 \left[\cos \left(\pi \frac{r}{2L_1} \right) u(L_1 - r) \right] \text{sech}^2 \left(\frac{z}{H_1} \right) \right\}, \end{aligned}$$

with $y_3 = -10$ pc, $z_3 = -20$ pc, $L_3 = 145$ pc, $H_3 = 26$ pc, $L_2 = 3.7$ kpc, $H_2 = 140$ pc, $L_1 = 17$ kpc and $H_1 = 950$ pc.

For the HIM, we turn again to Almy et al.'s (2000) hydrostatic-polytropic model. With $\langle n_{H^+} \rangle_{\text{HIM}} = \langle n_e \rangle_{\text{HIM}} / 1.2$, the H^+ space-averaged density of the HIM directly follows from Equation 14:

$$\langle n_{H^+} \rangle_{\text{HIM}} = \left\{ (0.009 \text{ cm}^{-3})^{2/3} - (1.54 \times 10^{-17} \text{ cm}^{-4} \text{ s}^2) \times [\phi(r, z) - \phi(0, 0)] \right\}^{1.5}, \quad (26)$$

where $\phi(r, z)$ is the Galactic gravitational potential of Wolfire et al. (1995) given by Equation 13.

For completeness, we also provide a description of the very hot medium detected by Koyama et al. (1989) and discussed at the end of section 2.4. Based on Yamauchi et al.'s (1990) and Koyama et al.'s (1996) studies, we assign to the VHIM an ellipsoid Gaussian density distribution with central electron density 0.35 cm^{-3} and FWHM size $(270 \text{ pc})^2 \times 150 \text{ pc}$. The major plane of the ellipsoid is seen edge-on from the Sun and tilted clockwise by 21° with respect to the Galactic plane, which leads us to introduce the coordinate transformation

$$\begin{cases} \eta = y \cos \alpha_{\text{vh}} + z \sin \alpha_{\text{vh}} \\ \zeta = -y \sin \alpha_{\text{vh}} + z \cos \alpha_{\text{vh}} \end{cases}, \quad (27)$$

with $\alpha_{\text{vh}} = 21^\circ$. The H^+ space-averaged density of the VHIM, $\langle n_{H^+} \rangle_{\text{VHIM}} = \langle n_e \rangle_{\text{VHIM}} / 1.2$, can then be written in terms of the (η, ζ) coordinates as

$$\langle n_{H^+} \rangle_{\text{VHIM}} = (0.29 \text{ cm}^{-3}) \exp \left[- \left(\frac{x^2 + \eta^2}{L_{\text{vh}}^2} + \frac{\zeta^2}{H_{\text{vh}}^2} \right) \right], \quad (28)$$

with $L_{\text{vh}} = 162$ pc and $H_{\text{vh}} = 90$ pc.

4.4. Altogether

The total space-averaged density of hydrogen nuclei in the interstellar GB is given by the sum of the partial contributions from the molecular, atomic and ionized media:

$$\langle n_{\text{H}} \rangle = 2 \langle n_{\text{H}_2} \rangle + \langle n_{\text{H}_\text{I}} \rangle + \langle n_{\text{H}^+} \rangle, \quad (29)$$

where

$$\langle n_{\text{H}_2} \rangle = \langle n_{\text{H}_2} \rangle_{\text{CMZ}} + \langle n_{\text{H}_2} \rangle_{\text{disk}} \quad (30)$$

(see Equations 18 and 23),

$$\langle n_{\text{H}_\text{I}} \rangle = \langle n_{\text{H}_\text{I}} \rangle_{\text{CMZ}} + \langle n_{\text{H}_\text{I}} \rangle_{\text{disk}} \quad (31)$$

(see Equations 19 and 24) and

$$\langle n_{\text{H}^+} \rangle = \langle n_{\text{H}^+} \rangle_{\text{WIM}} + \langle n_{\text{H}^+} \rangle_{\text{HIM}} + \langle n_{\text{H}^+} \rangle_{\text{VHIM}} \quad (32)$$

(see Equations 25, 26 and 28). For an assumed total-to-hydrogen mass ratio of 1.453 (see beginning of section 2), the total space-averaged mass density of interstellar gas in the interstellar GB is related to the above hydrogen space-averaged density through

$$\langle \rho \rangle = 1.453 m_{\text{P}} \langle n_{\text{H}} \rangle, \quad (33)$$

where m_{P} is the proton rest mass.

Displayed in Figure 6 is the radial variation of the azimuthally-averaged column densities through the

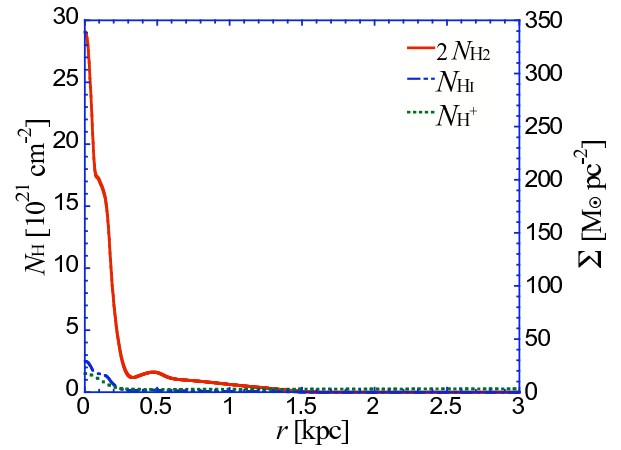


Fig. 6. Azimuthally-averaged column densities through the Galactic disk of interstellar hydrogen nuclei in molecular form (solid line), atomic form (dot-dashed line) and ionized form (dotted line) and associated surface densities of total interstellar matter (assuming a total-to-hydrogen mass ratio of 1.453; see section 2) as functions of Galactic radius.

Galactic disk of the molecular, atomic and ionized gases. The vertical variation of their hydrogen space-averaged densities is shown in Figure 7 at three representative horizontal locations, namely, at the GC $[(x, y) = (0, 0)]$, at the center of the CMZ $[(x, y) = (-50 \text{ pc}, 50 \text{ pc})]$ and at the point of the GB disk (projected onto the Galactic plane) where its major axis intersects its “ridge” $[r = \frac{3}{4}(1.47 \text{ kpc}), \theta = 47.6^\circ]$ (see below Equation 24), i.e., $(x, y) = (742 \text{ pc}, 815 \text{ pc})$. The graphs speak for themselves. The molecular gas (solid line) is by far the most abundant. Its radial distribution exhibits a high peak at the origin corresponding to the CMZ and a lower bump at $r \simeq 4.7$ kpc corresponding to the holed GB disk. Along the vertical, it is confined to a thin layer, which is nearly centered on the Galactic midplane, except outside the CMZ, where it is centered on the tilted midplane of the GB disk (see Figure 7c). The atomic gas (dot-dashed line) is about ten times less abundant than the molecular gas, it has virtually the same radial distribution and it occupies an approximately three times thicker layer. Finally, the ionized gas (dotted line) is the most rarefied, and it spreads much farther out in all directions. The slight rise in its radial distribution outside ~ 1 kpc is due to the contribution from the Galactic disk.

5. Conclusions

In this paper, we took stock of the present observational status of interstellar gas in the Galactic bulge (defined as the region interior to $r = 3$ kpc) and we discussed in some detail existing theoretical models of interstellar gas dynamics near the GC. We then provided simple analytical expressions for the hydrogen space-averaged densities of the different gas components that fit at best the observational data and are consistent with the theoretical predictions. All our expressions are written in parametric form, which will make them easy to update and adapt to future observations showing other characteristics (shape, dimensions, orientation, mass) than those adopted here. Our results are summarized in section 4.4.

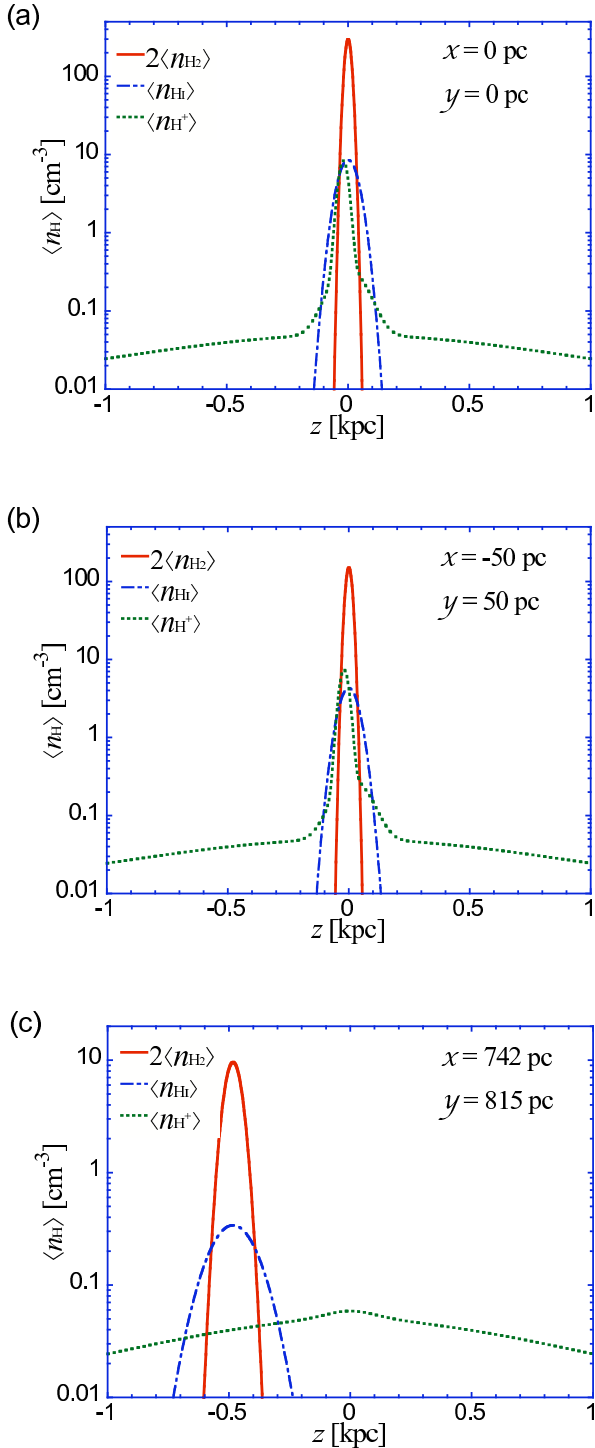


Fig. 7. Space-averaged densities of interstellar hydrogen nuclei in molecular form (solid line), atomic form (dashed line) and ionized form (dotted line) as functions of Galactic height: (a) at the GC; (b) at the center of the CMZ; (c) at the point of the GB disk (projected onto the Galactic plane) where its major axis intersects its “ridge”.

We did not address the issue of where our modeled interstellar gas would appear in an (l, v) or full (l, b, v) plot. Doing so would require studying the gas dynamics in a specified non-axisymmetric Galactic gravitational potential with a given pattern speed. This is undoubtedly a step that

should be taken in the future, especially as the (l, b, v) space is the one that observers have direct access to.

Aside from the space-averaged densities, we were able to gather some interesting observational information on the physical conditions (temperature and true density) in the molecular and ionized media. In section 2.2, we saw that the molecular medium probably contains a cold, high-density component with $T \sim 50$ K and $n_{\text{H}_2} \sim 10^{3.5-4} \text{ cm}^{-3}$, and a warm, low-density component with $T \sim 150$ K and $n_{\text{H}_2} \sim 10^{2.5} \text{ cm}^{-3}$. It is also possible that the temperature and true density in the molecular medium vary more-or-less continuously over broad ranges of values. In section 2.4, we were led to describe the ionized medium as the superposition of three components with radically different temperatures: the WIM with $T \sim 10^4$ K, the HIM with $T \sim$ a few 10^6 K and the VHIM with $T \gtrsim 10^8$ K. However, we were unable to obtain independent estimates for the associated true densities. As for the atomic medium, we may conjecture by analogy with the interstellar vicinity of the Sun that a cold and a warm phase co-exist, although we found little direct evidence to substantiate this hypothesis and even less direct quantitative information on the physical conditions in these two putative phases.

It would be highly desirable to estimate the filling factors of the different media. Unfortunately, this cannot be done in any meaningful way for the atomic and ionized media, whose true densities are not known. In contrast, crude upper limits can be derived for the two components of the molecular medium. Remember that the filling factor is by definition the ratio of space-averaged to true density. The H_2 space-averaged density attains its maximum value in the CMZ, where $\langle n_{\text{H}_2} \rangle_{\text{max}} = 150 \text{ cm}^{-3}$ (see Equation 18). If, as argued by Rodríguez-Fernández et al. (2001), $\sim 30\%$ of the interstellar molecular gas resides in the warm component (see section 2.2) and if the cold and warm components have true densities $\sim 10^{3.5-4} \text{ cm}^{-3}$ and $\sim 10^{2.5} \text{ cm}^{-3}$, respectively, then their filling factors are $\lesssim 3.3\%$ and $\lesssim 14\%$, respectively.

Acknowledgements. The authors would like to thank W.B. Burton, J. Cordes, F. Combes, T. Dame, R. Fux, R. Launhardt, J. Lazio, D. McCammon, C. Martin, N. McClure-Griffiths, N. Rodríguez, and the referee, J. Binney, for their helpful comments.

References

- Afflerbach, A., Churchwell, E., & Werner, M. W. 1997, *ApJ* 478, 190
- Almy, R. C., McCammon, D., Digel, S. W., et al. 2000, *ApJ* 545, 290
- Anders, A., & Grevesse, N. 1988, *Geochimica et Cosmochimica Acta* 53, 197
- Arimoto, N., Sofue, Y., & Tsujimoto, T. 1996, *PASJ* 48, 275
- Athanassoula, E. 1992, *MNRAS* 259, 328
- Athanassoula, E. 1992, *MNRAS* 259, 345
- Bally, J., Stark, A. A., Wilson, R. W., et al. 1987, *ApJS* 65, 13
- Bally, J., Stark, A. A., Wilson, R. W., et al. 1988, *ApJ* 324, 223
- Benjamin, R. A., Churchwell, E., Babler, B. L., et al. 2005, *ApJ* 630, L149
- Binney, J., Gerhard, O. E., Stark, A. A., et al. 1991, *MNRAS* 252, 210
- Binney, J., Gerhard, O., & Spergel, D. 1997, *MNRAS* 288, 365
- Binney, J., & Merrifield, M. 1998, in *Galactic Astronomy*, ed. J. P. Ostriker and D. N. Spergel (Princeton, New Jersey)
- Bitran, M. 1987, Ph.D. thesis, University of Florida
- Bitran, M., Alvarez, H., Bronfman, L., et al. 1997, *A&AS* 125, 99
- Bissantz, N., Englmaier, P., & Gerhard, O. 2003, *MNRAS* 340, 949
- Bissantz, N., & Gerhard, O. 2002, *MNRAS* 330, 591
- Burton, W. B., & Liszt, H. S. 1978, *ApJ* 225, 815
- Burton, W. B., & Liszt, H. S. 1992, *A&AS* 95, 9

- Burton, W. B., & Liszt, H. S. 1993, *A&A* 274, 765
- Carr, J. S., Sellgren, K., & Balachandran, S. C. 2000, *ApJ* 530, 307
- Combes, F. 1991, *ARA&A* 29, 195
- Contopoulos, G., & Mertzaniades, C. 1977, *A&A* 61, 477
- Contopoulos, G., & Papayannopoulos, Th. 1980, *A&A* 92, 33
- Cordes, J. M., & Lazio, T. J. W. 2002, *astro-ph/0207156*
- Cordes, J. M., Weisberg, J. M., Frail, D. A., et al. 1991, *Nature* 354, 121
- Dahmen, G., Hüttmeister, S., Wilson, T. L., et al. 1998, *A&A* 331, 959
- Däppen, W. 2000, in *Allen's Astrophysical Quantities*, ed. A. N. Cox (Springer-Verlag, New York), 27
- Ferrière, K. M. 1998, *ApJ* 497, 759
- Ferrière, K. M. 2001, *RvMP* 73, 1031
- Fux, R. 1999, *A&A* 345, 787
- Englmaier, P., & Gerhard, O. 1999, *MNRAS* 304, 512
- Heiligman, G. M. 1987, *ApJ* 314, 747
- Jenkins, A., & Binney, J. 1994, *MNRAS* 270, 703
- Kaifu, N., Kato, T., & Iguchi, T. 1972, *Nature* 238, 105
- Koyama, K., Awaki, H., Kunieda, H., et al. 1989, *Nature* 339, 603
- Koyama, K., Maeda, Y., Sonobe, T., et al. 1996, *Publ. Astron. Soc. Japan* 48, 249
- Launhardt, R., Zylka, R., & Mezger, P. G. 2002, *A&A* 384, 112
- Lazio, T. J. W. & Cordes, J. M. 1998, *ApJ* 505, 715
- Liszt, H. S., & Burton, W. B. 1978, *ApJ* 226, 790
- Liszt, H. S., & Burton, W. B. 1980, *ApJ* 236, 779
- Liszt, H. S., & Burton, W. B. 1996, in *Unsolved problems of the Milky Way*, Proceedings of the 169th IAU Symposium, ed. L. Blitz and P. Teuben (Kluwer, Dordrecht), 297
- Maciel, W. J., & Quireza, C. 1999, *A&A* 345, 629
- Magnani, L., Zelenik, S., Dame, T. M., et al. 2006, *ApJ* 636, 267
- Martin, C. L., Walsh, W. M., Xiao, K., et al. 2004, *ApJS* 150, 239
- Mehring, D. M., Yusef-Zadeh, F., Palmer, P., et al. 1992, *ApJ* 401, 168
- Mehring, D. M., Palmer, P., Goss, W. M., et al. 1993, *ApJ* 412, 684
- Mezger, P. G., Duschl, W. J., & Zylka, R. 1996, *Astron. Astrophys. rev.* 7, 289
- Mezger, P. G., & Pauls, T. 1979, in *The Large-Scale Characteristics of the Galaxy*, Proceedings of the 84th IAU Symposium, ed. W. B. Burton (Reidel, Dordrecht), 357
- Morris, M., & Serabyn, E. 1996, *ARA&A* 34, 645
- Najarro, F., Figer, D. F., Hillier, D. J., et al. 2004, *ApJ* 611, L105
- Oka, T., Hasegawa, T., Sato, F., et al. 1998, *ApJ* 493, 730
- Oka, T., Geballe, T. R., Goto, M., et al. 2005, *ApJ* 632, 882
- Rodríguez-Fernández, N. J., Martín-Pintado, J., Fuente, A., et al. 2001, *A&A* 365, 174
- Rohlfs, K., & Braunsfurth, E. 1982, *A&A* 113, 237
- Rolleston, W. R. J., Smartt, S. J., Dufton, P. L., et al. 2000, *A&A* 363, 537
- Sanders, D. B., Solomon, P. M., & Scoville, N. Z. 1984, *ApJ* 276, 182
- Sawada, T., Hasegawa, T., Handa, T., et al. 2004, *MNRAS* 349, 1167
- Scoville, N. Z. 1972, *ApJ* 175, L127
- Sellwood, J. A., & Sparke, L. S. 1988, *MNRAS* 231, 25
- Shaver, P. A., McGee, R. X., Newton, L. M., et al. 1983, *MNRAS* 204, 53
- Smartt, S. J., Venn, K. A., Dufton, P. L., et al. 2001, *A&A* 367, 86
- Snowden, S. L., Egger, R., Freyberg, M. J., et al. 1997, *ApJ* 485, 125
- Sodroski, T. J., Odegard, N., Dwek, E., et al. 1995, *ApJ* 452, 262
- Sofue, Y. 1995a, *PASJ* 47, 527
- Sofue, Y. 1995b, *PASJ* 47, 551
- Stark, A. A., Bally, J., Knapp, G. R., et al. 1988, in *Molecular Clouds in the Milky Way and External Galaxies*, ed. R. L. Dickman, R. L. Snell, and J. S. Young (Springer-Verlag, Berlin), 303
- Strong, A. W., Moskalenko, I. V., Reimer, O. et al. 2004, *A&A* 422, L47
- Taylor, J. H., & Cordes, J. M. 1993, *ApJ* 411, 674
- Wada, K. 1994, *PASJ* 46, 165
- Wolfire, M. G., McKee, C. F., Hollenbach, D., et al. 1995, *ApJ* 453, 673
- Yamauchi, S., Kawada, M., Koyama, K., et al. 1990, *ApJ* 365, 532